DARU Journal of Pharmaceutical Sciences (2020) 28:139–157
https://doi.org/10.1007/s40199-019-00325-9

RESEARCH ARTICLE

In Silico design of AVP (4–5) peptide and synthesis, characterization and in vitro activity of chitosan nanoparticles

Serda Kecel-Gunduz[1] · Yasemin Budama-Kilinc[2] · Rabia Cakir-Koc[2] · Tolga Zorlu[3,4] · Bilge Bicak[1,5] · Yagmur Kokcu[5] · Aysen E. Ozel[1] · Sevim Akyuz[6]

Received: 16 January 2019 / Accepted: 23 December 2019 / Published online: 16 January 2020

Abstract

Background Arginine-vasopressin (AVP) is a neuropeptide and provides learning and memory modulation. The AVP (4–5) dipeptide corresponds to the N-terminal fragment of the major vasopressin metabolite AVP (4–9), has a neuroprotective effect and used in the treatment of Alzheimer's and Parkinson's disease.

Methods The main objective of the present study is to evaluate the molecular mechanism of AVP (4–5) dipeptide and to develop and synthesize chitosan nanoparticle formulation using modified version of ionic gelation method, to increase drug effectiveness. For peptide loaded chitosan nanoparticles, the synthesized experiment medium was simulated for the first time by molecular dynamics method and used to determine the stability of the peptide, and the binding mechanism to protein (*HSP70*) was also investigated by molecular docking calculations. A potential pharmacologically features of the peptide was also characterized by ADME (Absorption, Distribution, Metabolism and Excretion) analysis. The characterization, in vitro release study, encapsulation efficiency and loading capacity of the peptide loaded chitosan nanoparticles (*CS NPs*) were performed by *Dynamic Light Scattering (DLS), UV–vis absorption (UV), Scanning Electron Microscopy (SEM), Fourier transform infrared (FT-IR) spectroscopy* techniques. Additionally, in vitro cytotoxicity of the peptide on human neuroblastoma cells (*SH-SY5Y*) was examined with XTT assay and the statistical analysis was evaluated.

Results The results showed that; hydrodynamic size, zeta potential and polydispersity index (PdI) of the peptide-loaded CS NPs were 167.6 nm, +13.2 mV, and 0.211, respectively. In vitro release study of the peptide-loaded CS NPs showed that 17.23% of the AVP (4–5)-NH2 peptide was released in the first day, while 61.13% of AVP (4–5)-NH2 peptide was released in the end of the 10th day. The encapsulation efficiency and loading capacity were 99% and 10%, respectively. According to the obtained results from XTT assay, toxicity on SHSY-5Y cells in the concentration from 0.01 μg/μL to 30 μg/μL were evaluated and no toxicity was observed. Also, neuroprotective effect was showed against H_2O_2 treatment.

Conclusion The experimental medium of peptide-loaded chitosan nanoparticles was created for the first time with in silico system and the stability of the peptide in this medium was carried out by molecular dynamics studies. The binding sites of the peptide with the *HSP70* protein were determined by molecular docking analysis. The size and morphology of the prepared NPs capable of crossing the blood-brain barrier (BBB) were monitored using DLS and SEM analyses, and the encapsulation efficiency and loading capacity were successfully performed with UV Analysis. In vitro release studies and in vitro cytotoxicity analysis on SHSY-5Y cell lines of the peptide were conducted for the first time.

Electronic supplementary material The online version of this article (https://doi.org/10.1007/s40199-019-00325-9) contains supplementary material, which is available to authorized users.

✉ Serda Kecel-Gunduz
skecel@istanbul.edu.tr

[1] Physics Department, Faculty of Science, Istanbul University, Vezneciler, 34134 Istanbul, Turkey

[2] Department of Bioengineering, Faculty of Chemical and Metallurgical Engineering, Yildiz Technical University, 34220 Istanbul, Turkey

[3] Graduate School of Natural and Applied Science, Yildiz Technical University, 34220 Istanbul, Turkey

[4] Department of Physical Chemistry and EMaS, Universitat Rovira i Virgili, 43007 Tarragona, Spain

[5] Institute of Graduate Studies in Sciences, Istanbul University, 34452 Istanbul, Turkey

[6] Physics Department, Science and Letters Faculty, Istanbul Kultur University, Atakoy Campus, Bakirkoy, 34156 Istanbul, Turkey

Keywords AVP (4–5) · Hsp70 · Drug delivery · Nanoparticle · Chitosan · Parkinson · MD

Abbreviations

AVP	Arginine-vaspressin
C S NPs	Chitosan nanoparticles
AD	Alzheimer's disease
PD	Parkinson's disease
NGF	Nerve growth factor
HSP	Heat shock proteins
MD	Molecular Dynamics
NVT	Number of particles, Volume, and Temperature
NPT	Number of particles, Pressure, and Temperature
Rg	Gyration
RMSD	Root mean square deviation
VMD	Visual Molecular Dynamics
ADME	Absorption, Distribution, Metabolism and Excretion
TED	Total energy distribution
PdI	Polydispersity index
FT-IR	Fourier Transform Infrared
SEM	Scanning Electron Microscopy
DLS	Dynamic Light Scattering
EE	Encapsulation Efficiency
LC	Loading Capacity
PBS	Phosphate Buffered Saline
XTT	sodium 3,3′-[1(phenylamino)carbonyl]-3,4-tetrazolium]-3is(4-methoxy-6-nitro) benzene sulfonic acid hydrate
DMSO	Dimethyl Sulfoxide

Background

Arginine-vasopressin (AVP), which acts like a growth factor, is a neuropeptide that plays important roles such as regulation of nephron recirculation, water contraction, cardiovascular functions, cognition, tolerance, adaptation and complex sexual or maternal behaviour in the body and modulating of learning and memory in human brain [1–3]. Degradation of the function or level of AVP hormone in the body with aging causes neurodegenerative diseases such as Alzheimer's (AD) and especially, Parkinson's disease (PD) [4]. Based on a clinical observation shows that the reduced AVP hormone secretion is also caused nocturia which is one of the commonest nonmotor symptoms in PD [5]. In an in vitro study which is conducted in 2006, it was predicted that the analog of arginine-vasopressin could be used in the treatment of (PD) [1]. The AVP (4–9) and AVP (4–8) are two different analogs of AVP which have the highest nootropic activity, however, have very low bioavailability. Due to this reason, the design of shorter dipeptides and tripeptide fragments of AVP, which can pass the blood-brain barrier (BBB) and the gastrointestinal tract with having high bioavailability, is of great importance to help to relieve of the symptoms of PD. On the other hand, AVP (4–5)-NH_2 (pGlu-Asn-NH_2) which is a short peptide chain is an important dipeptide that corresponds to N-terminal fragment of major vasopressin metabolite AVP (4–9), was synthesized with neuroprotective effect. In vitro studies which was carried out with mouse hippocampal neuronal cell line (HT-22) showed that when enough concentration of AVP (4–5)-NH_2 dipeptide interacted with neurotrophins and especially, heat shock protein 70 (HSP70) which plays critical role in the cell growth and survival in many organisms, the content of endogenous neuroprotective effects increased [1]. It is also known that Hsp70 is one of the important components of the cellular network and folding catalysts [6] and inhibits the formation of α-synuclein fibrils and β-amyloid during PD and AD, respectively. Because of over-expression of Hsp70, molecular chaperones suppress the toxicity of aberrantly folded proteins that occur in AD and PD [2, 7, 8].

In recent year, pharmaceutical researchers focused on the encapsulation of the active compounds into the biocompatible polymers. Polymer encapsulated systems provide long term released of active compounds like peptides, proteins or genes [9]. Among the polymers, chitosan is safe and non-toxic material used for encapsulation studies [10]. Chitosan [(1, 4)-2-amino-2-deoxy-D-glucan] (CS), a derivative of the chitin which is included in the shell of crustacean and the cell wall of fungi, is frequently used in medical field due to its high biocompatibility and non-toxic effects [11, 12]. In recent years, some studies which were carried out with the nanoparticular forms of CS (CS NPs) showed that this organic material can be used for delivery of various neuroprotective peptides in the body [13]. One of these studies, levodopa (L-DOPA) which is used for treatment of symptoms of PD was encapsulated in CS NPs and their cellular effects were observed on PC12 cells [14]. According to the results, L-DOPA-loaded CS NPs increased the cell viability as nearly 85% while this rate was only as nearly 43% for L-DOPA. These results showed that CS NPs is not only a drug delivery agent but also it has neuroprotective effects. In this way, various neuroprotective drugs or peptides can be easily delivered and their effectiveness can be amplified with CS NPs. Therefore, the AVP (4–5)-NH_2 dipeptide was encapsulated by using chitosan polymer for development of pharmaceutical formulation. The drug delivery system based on CS NPs was synthesized using modified version of ionic gelation method, to overcome low bioavailability and increase the peptide effectiveness. In addition, in vitro release profile of AVP (4–5)-NH_2 loaded CS NPs was performed against phosphate-buffered saline (PBS) at pH 7.4. Furthermore, in vitro cytotoxicity and neuroprotective effect of peptide and CS NPs on human

neuroblastoma cells (SH-SY5Y) was examined with a colorimetric method based on the tetrazolium salt (XTT).

In this study, the experimental medium of peptide-loaded chitosan nanoparticles was created for the first time with in silico system and the stability of the peptide in this medium was carried out by molecular dynamics studies. The active binding mechanism between AVP (4–5)-NH_2 and HSP70 protein was investigated using molecular docking method and a potent pharmacologically features of peptide were also emerged by ADME (Absorption, Distribution, Metabolism and Excretion) profile. The characteristic wavenumbers of the AVP (4–5)-NH_2 were observed in the experimental vibrational (IR and Raman) spectra together with the fundamental vibrational wavenumbers which were calculated at the level of DFT-RB3LYP / 6–31++G (d, p) basis set. Also, the assignments of the fundamental wavenumbers, which were calculated using the scaled quantum mechanical force field (SQM FF) method, were performed in accordance with the total energy distribution of the vibrational modes (TED).

Methods

Materials

AVP (4–5)-NH_2 dipeptide was purchased from GL-Biochem Co. CS (Low Molecular Weight) (Cat No: 448869), and triphenylphosphate (TPP) (Cat No: 241288) were purchased from Sigma–Aldrich (USA). Acetic acid (Cat No: 1.00056.2500) was purchased from Merck Millipore (100%) (Darmstadt, Germany). DMEM-F12 Medium, Fetal Bovine Serum and Penicilum–Streptomycin were obtained from Gibco. XTT was obtained from Invitrogen. Ultrapure water from Millipore Milli-Q Gradient System was used to prepare the solutions for synthesis and cell culture experiments.

Instrumentation

The NPs were prepared with ultrasonic horn (Bandelin, Sonopuls) and centrifuge (Hettich, Germany). The absorption spectra were obtained from UV-Vis spectrometer (Shimadzu, Japan) for used in preparation of calibration curve of in vitro release study of AVP (4–5)-NH_2 peptide. Hydrodynamic size, polydispersity index (PdI) and zeta potential values were obtained from Zeta-Sizer Nano ZS (Malvern Instruments, Malvern, UK). Scanning Electron Microscopy (SEM) (Zeiss Gemini 500) was used to observation of the morphology of AVP (4–5)-NH_2 peptide-loaded CS NPs. Fourier-transform infrared (FT-IR) spectra were recorded using a Jasco 6300 FT-IR. In order to measure the cell viability, Microplate Photometer (Thermo Labsystems Multiskan Ascent 354) was used.

Molecular dynamics simulations

Firstly the optimized molecular geometries of the AVP (4–5)-NH_2, chitosan, acetic acid, TPP (tripolyphosphate) molecules which are used at experimental step have been obtained by using the Gaussian16 software [15]. To obtain the parameters and topologies that belong to the molecules, some specific programs and tools were used [16–19]. After all topology and parameter files were generated for the peptide, (MD) simulation step was carried out. MD simulation was performed by GROMACS 2016.1 [20] program using AMBER99SB force field [21].

In the first system, AVP (4–5)-NH_2 peptide was put in a cubic box that was filled with 751 water molecules using TIP4P water models [22] and then MD study was realized for comparing with other system. In the second system, AVP (4–5)-NH_2 molecule was put in a cubic box including 30 chitosan molecules, 5 acetic acid and 5 TPP and then, the box was filled with 30,259 water molecules using TIP4P water models and added 12 Na^+ ions to neutralize the net charge of the system. The energy minimization of systems was achieved using 50,000 steps of steepest descent algorithm. For equilibrations, the systems were stabilized at 310 K using V-rescale thermostat for 100 ps as NVT ensemble [23] and Parrinello-Rahman pressure-coupling with 1.0 bar pressure [24] for 100 ps as NPT ensemble. After the resulting ensembles, 5 ns MD simulations were run with 2 fs time step for each simulation. During simulations, LINCS algorithm [25] was used for constraining the bond length. The graphics were plotted using XMGRACE [26] and VMD was used for the visualization of the box [27].

Molecular docking and ADME analysis

Firstly, the protein used for the docking study was selected from PDB databank (PDB code: 1S3X) [28] and its homology model was obtained by the SWISS-MODEL [29] server for better results. Taking the molecular structure from the result of MD simulation, the preparation and calculations of molecular docking was done by Schrödinger Maestro software using the Glide SP (standard precision) module (Schrödinger Release 2017–4: Maestro, Schrödinger, LLC, New York, NY, 2017) [30–32].

Firstly, AVP (4–5)-NH_2 as a ligand molecule was prepared for docking calculations by the LigPrep tool in the Maestro 11.4 version of the Schrödinger Software program using the OPLS3 force field [33]. The 32 stereoisomers were produced for the ligand after the ionization states at pH 7.0 ± 2.0 which were selected. The structure of selected receptor of Heat Shock 70 kDa protein 1

having a solubility of 1.84 Å was prepared by the Protein Preparation Wizard tool [34]. The polar hydrogens were added to the heavy atoms and all waters and ions in the structure were removed. The bond orders were assigned, charges were defined at pH 7.0 and the selected receptor was optimized using PROPKA [35]. The heavy atoms in the receptor were converged by preferring 0.3A° RMSD and the OPLS3 force field. The Grid box was defined to the receptor by centering the existing co-crystallized ligand using grid generation tool in Maestro 11.4 version. The ligand was docked into the receptor based on the grid using standard precision (SP) docking algorithm to rank the ligand with specific conformation of the receptor molecule [36]. Drug candidate molecules display favourable ADME parameters. The Qik-Prop module (Schrödinger Release 2017–4: QikProp, Schrödinger, LLC, New York, NY, 2017.) was used to determine the ADME profile of the drug candidate molecule.

FT-IR analysis

The FT-IR spectra for AVP (4–5)-NH_2 loaded CS NPs were recorded on a Jasco FT/IR-6300 spectrometer with diamond ATR unit in the range 400–4000 cm^{-1} and 2 cm^{-1} resolution. The GRAMS/AI 7.02 (Thermo Electron Corporation) software package was used to provide the baseline adjustment, second derivative (Savitzky–Golay function with 2 polynomial and 9 points), and peak fitting which is used band component analysis procedure. The Raman spectrum of the sample was taken with a Jasco NRS-3100 micro-Raman spectrometer (1200 lines/mm grating and high sensitivity cooled CCD).

Preparation of AVP (4–5)-NH_2 peptide loaded CS NPs

CS NPs were prepared using a simple ionic gelation process with some modifications as described elsewhere [37–40]. Optimization studies were conducted, and the effects of the concentration of chitosan, TPP and peptide to particles size, polydispersity index and zeta potential values were investigated. Finally, optimum preparation method was determined. Briefly, 2 mg of CS were dissolved in 10 mL of 0.33% of acetic acid solution under magnetic stirring at 55–60 °C for an hour. Then, the solution was sonicated another 1 h for completely dissolving of CS in the solution. Notably, dissolving of CS in aqueous medium is very difficult. For this reason, sonication process is essential. Finally, the pH of the solution was adjusted to 4.7 with aid of 0.1 M of NaOH. On the other hand, 10 mL of aqueous TPP solution (1.53 mM) was prepared and stored at +4 °C for further use. For synthesis of CS NPs, 3.3 mL of ice-cold TPP solution was injected to 10 mL of CS at 4 °C under magnetic stirring. After 10 min later, white turbidity was observed, and this indicated that CS NPs were successfully obtained. For the synthesis of AVP (4–5)-NH_2 peptide-loaded CS NPs, same amounts and the method which is described above were used. However, to prepare of the peptide loaded CS NPs, 2 mg AVP (4–5)-NH_2 peptide were dissolved in 1 mL of ethanol (EtOH) and mixed with 20 mL CS solution which include 0.33% acetic acid. After the mixing, 6.6 mL of TPP solution injected to this solution at 4 °C.

Dynamic light scattering (DLS) analysis

In order to determine the physicochemical properties of the NPs in the aqueous medium, DLS measurements were used. Every electrophoretic light scattering measurement was performed at 25 °C with 4.0 mW He-Ne laser operating at a wavelength of 633 nm. Hydrodynamic size, zeta potential, and PdI values were reported as the mean of at least five determinations.

Preparation of calibration curve of AVP (4–5)-NH_2 peptide

The calibration curve was constructed with standard solutions of AVP (4–5)-NH_2 peptide absorbance values were recorded at 217.2 nm. This curve was used for quantification for further encapsulation efficiency and loading capacity studies.

Encapsulation efficiency and loading capacity of AVP (4–5)-NH_2 peptide loaded CS NPs

UV-Vis spectrometer was used to determine the encapsulation efficiency and loading capacity of AVP (4–5)-NH_2 peptide.

The EE and LC were calculated as follows:

$$EE\% = \frac{(The\ Total\ Peptide - Free\ Peptide)}{The\ Total\ Peptide} \times 100\% \quad (1)$$

$$LC\% = \frac{(The\ Total\ Peptide - Free\ Peptide\ )}{Total\ Amount\ of\ the\ Nanoparticles\ Weight} \times 100\% \quad (2)$$

In vitro release of AVP (4–5)-NH_2 peptide-loaded CS NPs

In vitro release study of the NPs was performed in PBS at pH 7.4 by dialysis method. Briefly, 1 mg/mL of AVP (4–5)-NH_2 peptide-loaded CS NPs were sealed with a cellulose membrane (10 kDa cut-off value) in a dialysis capsule. The whole system was maintained at 37 °C and kept in a water bath shaker. During the release process, 1 mL of dialysis medium was used at a predetermined time point (0, 0.5, 1, 2, 3, 4,

5, 6, 7, 8, 9, 10, 24, 48, 96, 120, and 240 h) while adding the same volume of fresh PBS. The released drug concentrations in each time points were determined as detailed in the following equation via UV–Vis spectrometer analysis.

$$\text{Release}\ (\%) = \frac{\text{Released Peptide}}{\text{Total Peptide}} \times 100\% \quad (3)$$

Scanning electron microscopy (SEM) analysis

The morphology of AVP (4–5)-NH_2 peptide-loaded CS NPs was analysed using SEM (Zeiss Supra 50 V). In order to increase the conductivity of the samples, 8.10^{-1} mbar / Pa vacuum was applied and 100 Å thickness gold-palladium (20–80%) plating was performed via Leica EM ACE600 device. The imaging was conducted using an accelerating voltage of 3 and 7 kV and with the 30 k times magnification.

Culture of SHSY-5Y cell line

SHSY-5Y (Neuroblastoma) cell line was used for cytotoxicity experiments (ATCC, Manassas, VA, USA). SHSY-5Y cells were seeded in 25 cm^2 cell culture flasks in DMEM-F12 Medium (Gibco,11320074) supplemented with Fetal Bovine Serum 10% (FBS-Gibco, 10500064) and Penicillium–Streptomycin (Gibco,15140122) 0.5% from 10,000 unit/mL Penicillin −10 mg/mL Streptomycin). Cells were incubated at 37 °C in 5% CO_2 until they reach 80% confluency. Then trypsinization was performed to remove cells from flask surface. After trypsinization, medium was added to the cells and centrifuged at 1000 rpm for 5 min. After centrifugation, the supernatant was removed, and cells were counted via a hemocytometry.

Treatment of AVP (4–5)-NH2, chitosan NPs, and AVP (4–5)-NH2 loaded chitosan NPs to SHSY-5Y cells

In vitro cytotoxicity assay was conducted on SHSY-5Y cell lines. The cells were seeded in 96 well flat bottom microplate with density of 1×10^4 cells for each well and incubated at 37 °C in 5% CO_2 incubator for 24 h. Then, cells were treated with different dilutions (2, 8, 32, 48, and 64 μg/μL) of AVP (4–5)-NH_2, Chitosan NPs, and AVP (4–5)-NH_2 loaded Chitosan NPs. After 24 h of incubation, the medium was aspirated and 100 μL of 0.5 mg/mL 2,3-bis-(2-methoxy-4-nitro-5-sulfophenyl)-2 H-tetrazolium-5-carboxanilide (XTT) solution (with 7.5 μg/mL phenazine methosulfate) in fresh medium were added to each well. The plate was incubated for 4 h at 37 °C in 5% CO_2 incubator [41]. The absorbance at 450 nm were read by multiplate reader (Labline). Percentage of cell viability was calculated with this formula;

$$\%cell\ viability = \frac{absorbance\ of\ test\ sample}{absorbance\ of\ control} \times 100 \quad (4)$$

Evaluation of neuroprotective effect in vitro

Neuroprotective effects of AVP (4–5)-NH_2, Chitosan NPs, and AVP (4–5)-NH_2 loaded Chitosan NPs on SH-SY5Y cells were examined. Briefly, SH-SY5Y cells were seeded in 96-well plates and incubated 24 h at 37 °C in 5% CO_2 incubator. After that 32 μg/μL AVP (4–5)-NH_2, Chitosan NPs, and AVP (4–5)-NH_2 loaded Chitosan NPs were separately added to the wells. After 24 h, medium was discarded, and cells were treated with 1,5 M of H_2O_2 for 30 min [1]. Medium was discarded again and XTT method were applied for assay cell viability as mentioned before. Non-treated cells were used as positive control and % cell viability calculated via Eq. 4.

Statistical analysis

Statistical comparisons were performed by unpaired Student's t test assuming equal variance for cytotoxicity assay. Differences were considered as statistically significant at $p \leq 0.05$. Data are the mean ± standard error (SE).

Results and discussion

Molecular dynamics results

Firstly, all molecules were placed into the cubic box that was filled with 30,259 water molecules using TIP4P water model (Fig. 1). The net charge of the system was neutralized with counter ions. In this study, 12 Na^+ ions were added to system for neutralization. For pH adjustment, NaOH were added to chitosan solution in the synthesis studies that were done using the ultra-pure water. According to this process, Na atoms were already available at preparation step of chitosan solution besides neutralization in the molecular dynamics study. After the system was completely constructed, the energy minimization was done using steepest descent algorithm. In energy minimization step, the potential energy of system was converged at 1120 steps with -1.5955162×10^6 kj/mol (Fig. S1). For equilibrations, NVT was achieved for 50,000 steps with a 2 fs time step at 310 K using the V-rescale thermostat that is a modified Berendsen thermostat and after NPT simulation at 1 bar result, the system's average density was obtained as 1000.34 kg/m^{-3} in (Fig. S2). Lately, MD simulation of molecule with 2,500,000 steps

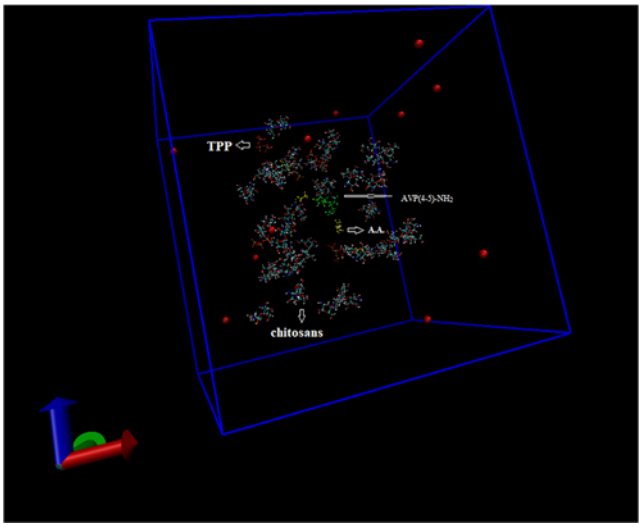

Fig. 1 The initial confirmation of the system and *counter ions* in a cubic box

was carried out for 5 ns. According to MD simulation, the average total, kinetic and potential energies were obtained at -1.14566×10^6 kj/mol, 2.39020×10^5 kj/mol and -1.38807×10^6 kj/mol, respectively (Fig. S3 and Fig. S4). When the system was compared with MD study of AVP (4–5)-NH_2 peptide in aqueous medium, it was observed that potential and total energies decreased while kinetic energy increased. The range of RMSD that belong to AVP (4–5)-NH_2 peptide in the system was seen under 0.2 nm changed from 0.0004880 to 0.1893775 for 5 ns while the RMSD range of the peptide in the aqueous medium ranged from 0.0005046 to 0.1024015. According to these results, it was determined that the structure of AVP (4–5)-NH_2 did not change significantly (Fig. 2). These RMSD values were important for verifying the stability of the structure. The MD study was given the preliminary information about stability of the peptide that exposed to the effects of other molecules in the synthesis of peptide loaded nanoparticles. Although molecular dynamics studies of various AVP derivatives have been performed in the literature [42, 43], there are no MD studies that simulate synthesized peptide loaded chitosan nanoparticles used in the experimental medium.

Molecular docking and ADME results

Molecular interaction and docking studies are very important for computer aided drug design and are used to better rationalize the action and prediction of the binding modes of drug candidate molecules. After the protein having 382 sequence length interacted with ligand, the energy of the docking score for AVP (4–5)-NH_2 peptide obtained as −8.205 kcal/mol (Table 1 and Fig. 3). The binding regions of the Hsp70 kDa protein 1 for AVP (4–5)-NH_2 were shown with hydrophobic interactions of **TYR15, CYS17** and polar residues of **THR14, THR13, THR204, SER16, SER340**. The hydrogen bonds that linked to the ligand to the receptor which were observed on the binding regions are **THR14 (1.86 Å and 2.19 Å)**, **LYS271 (2.36 Å), GLY339 (2.42 Å and 2.01 Å)** and **ASP366 (2.42 Å)**, respectively (Fig. 3a**.**, **3b., 3c.**). The electrostatic potential map surfaces of the ligand and receptor protein were also constituted to define the regions that were electron-rich and electron-poor (Fig. S5). Moreover, favourable ADME properties which explain the pharmacological properties of a molecule that are necessary for being a drug candidate obtained using Qikprop tool of the Maestro software package and tabulated in Table 2. Lipinski's five rules are used to determine whether the molecule having a pharmacological or biological activity, which has chemical and physical properties that make it an active drug. Lipinski's rule generally refers to values that are multiples of 5, and generally an active drug must accomplish the following criteria [44, 45]. According to these rules, the molecular weight (mol_MW) of the drug candidate molecule should be less than 500 Da. The calculated molecular weight was 242.234 g/mol and is among the recommended values (recommended from 725 to 130). For a molecule of drug candidate, an octanol-water partition coefficient (log P) should not be greater than 5 [46]. Especially, logP coefficient, as one of estimative factors for BBB (Blood-Brain Barrier) [47], is crucial for the peptide having neuroprotective properties. The value of octanol-water partition coefficient that belongs to peptide was −4.023.

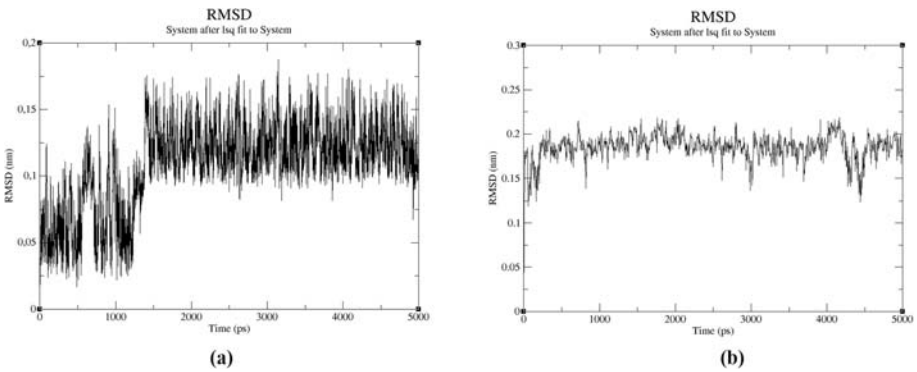

Fig. 2 RMSD values of AVP(4–5)-NH_2 peptide in aqueous medium (**a**) and in the system (**b**)

Table 1 The conformation and docking score energies of **AVP(4–5)-NH_2**

Ligand	Energy(kcal/mol)	Docking Score(kcal/mol)
1	3.340	−8.205
2	−1.918	−8.204
3	4.229	−8.182
4	−1.255	−7.098

According to these rules, the drug candidate molecule must have 5 hydrogen bond donors (total nitrogen-hydrogen and oxygen-hydrogen bond). The sum of the NH and OH bonds gives the number of hydrogen bond donors and the sum of the N and O atoms in the structure gives the number of hydrogen bond acceptors. In this molecule; there are four oxygen atoms which formed at least one hydrogen bond with **THR14, LYS271, SER340 and GLY339,** two NH groups and two NH_2 active groups which formed one hydrogen bond with **ASP366** that make hydrogen bonds with the protein and shown in Fig. 3c**.** Also calculated value for solute as donor-hydrogen bonds was 4.250 (recommended from 0 to 6). In addition, up to 10 hydrogen bond receptors (all nitrogen or oxygen atoms) must be present in the molecule and the measured value of the molecule according to ADME is (8.250) again among the recommended values (from 2.0/ to 20.0). In addition to these rules, the polar surface area (PSA) and the number of routable bonds is two of the defining characteristics of the active drug determination and selection process. The active drug should have 10 or less routable bonds and the polar surface area should not be greater than 140 $Å^2$ [48]. For AVP (4–5)-NH_2 peptide, the number of rotatable bonds is 8 and the polar surface area is measured as 180,528 $Å^2$ (Table 2). BBB permits diffusion of hydrophobic molecules and small polar molecules, while restricts the dissolution of bacteria and large

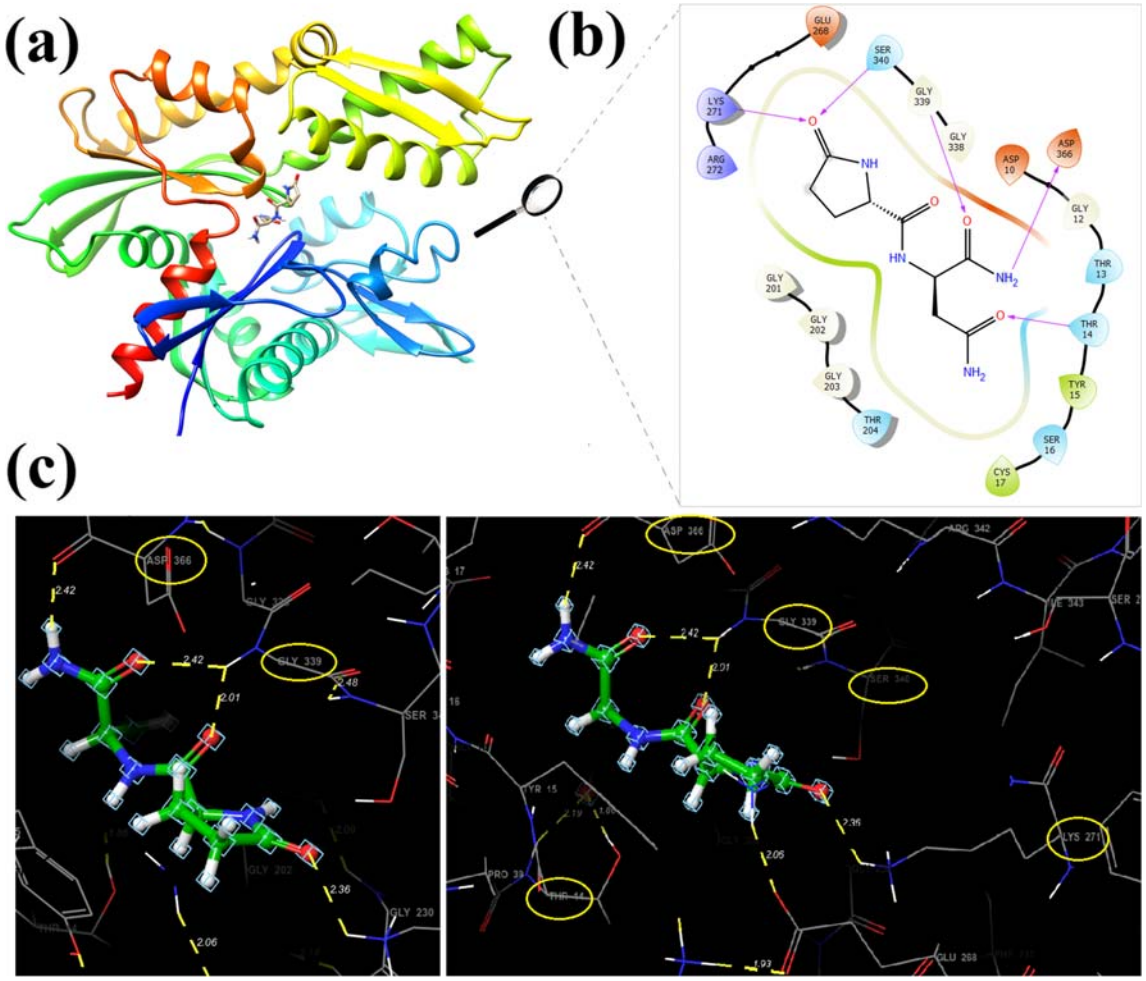

Fig. 3 The binding poses between that active site of Hsp70 Receptor and AVP(4–5)-NH_2 peptide (**a**), 2D ligand interaction of AVP(4–5)NH_2 peptide in the active side of the protein (**b**), the binding interaction of AVP(4–5)-NH_2 peptide with THR14 (1.86 Å and 2.19 Å), LYS271 (2.36 Å), GLY339 (2.42 Å AND 2.01 Å) and ASP366 (2.42 Å) residues of protein, respectively

Table 2 Docking score and calculated ADME properties of AVP(4–5)-NH_2 peptide

Property	Value	Recommended
Docking score (kcal/mol)	−8.205	
Polar surface area PSA (A°2)	180.528	(7.0 / 200.0)
Molecular weight MW (g/mol)	242.234	(130.0 / 725.0)
Solute as Donor-Hydrogen Bonds	4.250	(0.0/ 6.0)
Solute as Acceptor-Hydrogen Bonds	8.250	(2.0/ 20.0)
Solute Ionization Potential (eV)	9.382	(7.9/ 10.5)
Solute Electron Affinity (eV)	−0.740	(−0.9/ 1.7)
Polarizability (Angstroms^3)	21.554 M	(13.0 / 70.0)
QP log P for hexadecane/gas	8.503 M	(4.0 / 18.0)
QP log P for octanol/gas	20.896 M	(8.0 / 35.0)
QP log P for water/gas	25.811 M	(4.0 / 45.0)
QP log P for octanol/water	−4.023	(−2.0 / 6.5)
QP log S for aqueous solubility	2.000	(−6.5 / 0.5)
QP log S - conformation independent	1.220	(−6.5 / 0.5)
QP log K hsa Serum Protein Binding	−2.059	(−1.5 / 1.5)
QP log BB for brain/blood	−2.516	(−3.0 / 1.2)
No. of Primary Metabolites	6	(1.0 / 8.0)
Predicted CNS Activity (−- to ++)	–	
HERG K+ Channel Blockage: log IC50	1.823	(concern below −5)
Apparent Caco-2 Permeability (nm/s)	0	(<25 poor. >500 great)
Apparent MDCK Permeability (nm/s)	3	(<25 poor. >500 great)
QP log Kp for skin permeability	−6.820	(Kp in cm/h)
Jm. max transdermal transport rate	3.665	(micrograms/cm^2-h)
Lipinski Rule of 5 Violations	1	(maximum is 4)
Jorgensen Rule of 3 Violations	1	(maximum is 3)
% Human Oral Absorption in GI (+ − 20%)	0	(<25% is poor)

or hydrophilic molecules in the blood into the cerebrospinal fluid (CSF) [49]. Neuroprotective drugs targeting the central nervous system must first cross BBB [50]. The corresponding value calculated by ADME is −2.516 recommended value range (−3.0 / 1.2). Additionally, solute electron affinity, solute ionization potential (IP (eV)) were also taken from the result of Qikprop analysis as −0.740 eV (standard limits from −0.9 to 1.7), 9.382 eV (standard limits from 7.9 to 10.5), respectively. It is presented in some oral prodrugs such as *dirithromycin, tacrolimus, saquinavir, ceftidoren*, *efonidipine* which do not have the expected molecular weight and PSA values [51]. In this study, AVP (4–5)-NH_2 peptide having some drug-like properties was showed that have acceptable for molecular weight and BBB value for drug candidate.

FT-IR analysis results

The typical absorption bands of CS are given in Table 3**.** The broad absorption peak at 3445 cm^{-1} and the prominent peaks at 1638 and 1558 cm^{-1} correspond to the O-H stretching and the C=O stretching for amide I and N-H bending for amide II vibrations, respectively and are marked in Fig. 4**.** The bands at 1412 and 1338 cm^{-1} were assigned to C-C-H bending. The C-N and C-O stretching vibrations were also seen at 1319 cm^{-1} and 1052; 1020 cm^{-1} for CS. The bands which are originated from TPP *(P=O) (O-P-O)* were also observed at 1126 and 929 cm^{-1}. The observed and assigned peaks for the polymer are compatible with the literature [38, 52–57].

In present study, the characteristic wavenumbers of the AVP (4–5)-NH_2 peptide, observed in the experimental vibrational (IR and Raman) spectra are given in Table 4, together with the fundamental vibrational wavenumbers, calculated at the level of DFT-RB3LYP / 6–31++G(d,p) basis set. The assignment of the Vibrational wavenumber was performed in accordance with the total energy distribution of the vibrational modes (TED), that was calculated using the scaled quantum mechanical force field (SQM FF) method [58], with the aid of scaled vibrational wavenumbers using dual scaling factors [59]. The major IR peaks at 3378 cm^{-1}; 3272 cm^{-1} and 3196 cm^{-1}; 2992 cm^{-1}

Table 3 The FT-IR spectrum of Chitosan polymer, AVP(4–5)-NH_2 peptide and AVP(4–5)-NH_2 peptide-loaded CS NPs

	Chitosan (CS)								AVP(4–5)NH_2			NPs
	FTIR					ATR		FTIR		FTIR		AVP(4–5)NH_2 CS NPs
	References							This Study				
Assignment of Chitosan	[51]	[52]	[53]	[54]	[55]	[56]	[38]	This Study	Assignment of PgluAsn NH_2	νexp.	νcal.	νexp.
O-H stretching	3500–3300	3367	3800–3000	3290; 3285	3750–3000	3500–3200		3445; 3293	*O-H stretching*	–	–	3445; 3292
NH stretching							–		*NH stretching*	3378;3272	3372;3320	
C-H stretching	–	2927	2867	2867	2920;2875	2865	–		*C-H stretching*	3196;2992	3001;2991	3180
CO stretching; NH_2 bending	1650;1600	1637;1559	1656;1554	1568	1645;1574	1650;1542	1635; 153-0	1638; 15581-542	*CO stretching (amide-I)*	**1697***	1680	**1696***
									H-N-H bending	**1648***	1591	**1646***
									C-N-H bending(amid-e-II)	**1534****	1524	**1534****
C-C-Hbending					1426;1375			1412; 1338	*H-C-H bending*	1458;1436	1472;1438	1474;1456
C-N stretching+ ν_s(-CH3)	1317		1322	–	1313	–	–	1319	*C-C-H bending*	1306;1268 1246; 1203 1130	1312;1263 s1247;1199 1139	1339;1320; 1124
C-O stretching; O-C-H bending					1261			–	*C-C_{PGLU} stretching;*	980;900	994;900	-;902
COC asym. Stretching	1150	1154	–	1152;1148	1150;	–	1153	–	*C-C_{ASN} stretching;*	932;879	923;870	928
C-O-C;C-O-H (CO stretching)	–	1081	1107	1081; 1060	1080;1065;1025	- 1027	1083; 103-1	- 1052; 1020	*C-C-N-H torsion*	669;615; 501	691;611; 495	642;626 519;473
Saccharide structure	–	897	–	892	890	–	–					
TPP (P=O) (O-P-O)	1170			–	–	1126;875	- 912	1126; 929				

* The result of band component analysis for amide-I (in Fig.5)

** The result of band component analysis for amide-II (in Fig.6)

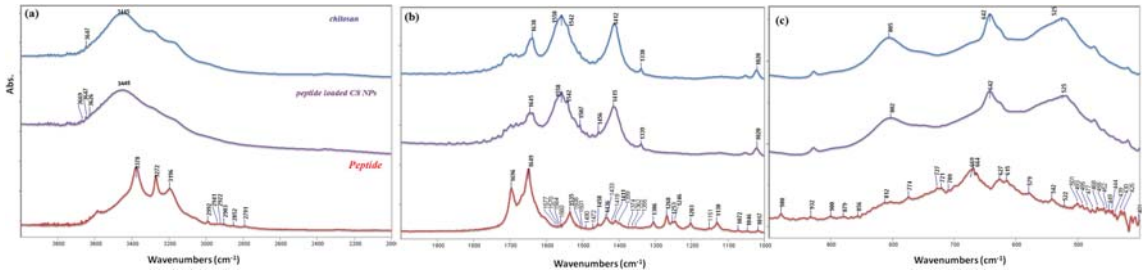

Fig. 4 The FT-IR spectrum of Chitosan polymer, AVP(4–5)-NH_2 peptide and AVP(4–5)-NH_2 peptide-loaded CS NPs in the range of 4000 cm^{-1} - 2000 cm^{-1}(**a**), 2000 cm^{-1} -1000 cm^{-1}(**b**), 1000 cm^{-1} -400 cm^{-1} (**c**)

indicate N-H and C-H stretching in FT-IR spectrum, respectively. The primary amide vibrations were appointed to **1696 cm^{-1}(IR)** and **1535 cm^{-1} (IR)** which characterized to amide-I and amide-II for AVP (4–5)-NH_2 peptide. In the present study, the C=O stretching in peptide group (amide-I) which was calculated and assigned by TED contributions (77% C=O stretching, 5% C-N stretching, 3% C-N-H bending) and observed in the 1715–1610 cm^{-1} and 1705–1610 cm^{-1} intervals for AVP(4–5)-NH_2 peptide and nanoparticle spectra, respectively.

The band component analyses of the amide-I and amide II regions of the IR spectra of the peptide and peptide loaded CS NPs were shown in Figs. 5 and 6, respectively. The C=O, amide-I and -II bands of the AVP(4–5)-NH_2 peptide were clearly shown in the IR spectrum of CS NPs, indicating the presence of the peptide in CS NPs. Due to the encapsulation of the AVP (4–5)-NH_2 peptide in CS NPs, slight wavelength and intensity changes occurred in both CS and peptide bands. Alterations of the amide I and II bands of the peptide can also be resulted due to the conformational alteration of the peptide after encapsulation. The peak observed at **1535 cm^{-1},** in the experimental FT-IR spectrum (see Fig. 6), was calculated at 1524 cm^{-1} and was assigned to the amide-II band of the peptide group by the help of TED analysis results ($\delta_{CNH}(51) + \upsilon_{CC}$ (4) + $\upsilon_{CN}(30) + \delta_{OCN}(3)$). The main H-N-H scissor vibration for ASN residue was assigned to 1649 cm^{-1} and the H-C-H scissors vibrations for PGLU and ASN moiety were assigned to 1458 cm^{-1} and 1436 cm^{-1} respectively, by the aid of TED (see Table 4).

The wagging and twisting vibrations for PGLU moiety were observed at 1268 cm^{-1} and 1203 cm^{-1}; 1130 cm^{-1}, whereas the wagging vibration for ASN moiety was observed at 1246 cm^{-1}. The band at 1306 cm^{-1} was denominated to C-C-H bending for PGLU. The peaks at 980 cm^{-1}, and 900 cm^{-1} corresponded to C-C stretching of PGLU, while the peaks at 932 $cm^{-1}$and 879 cm^{-1} complied with C-C stretching of ASN moiety. The C-C-N-H torsion vibrations were also identified at 669, 615 and 501 cm^{-1}.

DLS results

Among the different nanomaterial characterization techniques, DLS is the one of crucial and useful method to evaluate particle size, size distribution, and the zeta potential of nanomaterials in solution [60]. In this way, we can understand how to act of our synthetic drug transport agent in the liquid and learn about the hydrodynamic size. In Fig. 7a, b, the average hydrodynamic size, zeta potential and polydispersity index (PdI) values of blank CS NPs are given as 60.23 nm, +11.3 mV and 0.219, respectively. It was found that the AVP (4–5)-NH_2 peptide-loaded CS NPs have a narrow size distribution with 0.211 and 167.6 nm average particle size as given in Fig. 7c. On the other hand, As seen from the Fig. 7d, the zeta potential value of AVP (4–5)-NH_2 peptide-loaded CS NPs are +13.2 mV. The results indicated that both blank CS NPs and AVP (4–5)-NH_2 peptide-loaded CS NPs are stable in the liquid because they are more resistant to aggregation due to their high zeta potential.

These results coincide with other previous studies. One of these studies, optimization and evaluation of doxorubicin (DOX) loaded CS NPs were investigated [61]. The result of this study, zeta potential of CS NPs was found as +8.35 mV and it was reported that there was not any agglomeration in solution of CS NPs. On the other hand, in our study, zeta potential values of blank CS NPs and AVP (4–5)-NH_2 peptide-loaded CS NPs were nearly 1.3 or 1.5 fold higher than +8.35 mV, respectively and therefore, we can say that both NPs have higher stability in the liquid medium. The effects of chitosan concentration, TPP concentration and peptide concentration to particle size, polydispersity index and zeta potential values were also investigated and tabulated in Table S1, Table S2 and Table S3, respectively. According to the conditions tested, there is a relationship between increased particle size and increased concentrations of chitosan and TPP, as well as the pH of the solution is effective on the stability of the nanoparticle system [62, 63].

Encapsulation efficiency and loading capacity results

The encapsulation and loading efficiency are the two crucial indices for the evaluation of nanocarrier systems.

Table 4 Experimental (IR, Raman) and calculated wavenumbers (cm^{-1}), and the TED of the vibrational modes of the **AVP(4–5)NH$_2$**

	Assign.	IR	Raman	DFT-RB3LYP 6-31G++(d,p)			DFT-RB3LYP 6-31G(d,p)			DFT-RB3LYP 6-31G(d)			†TED-MONOMER DFT-RB3LYP 6-31G++(d,p)
		υ_{exp}	υ_{exp}	υ_{cal}	*υ_{scaled}	*IRint.*	υ_{cal}	*υ_{scaled}	*IR int.*	υ_{cal}	*υ_{scaled}	*IR int.*	
1	υ_{N}*asymm.*			3736	3568	45	3745	3576	40	3719	3552	36	υ_{NH} (100)
2	υ_{NH}*asymm.*			3682	3516	103	3685	3519	89	3662	3497	80	υ_{NH} (100)
3	υ_{NH}*pglu*			3615	3453	30	3627	3464	28	3606	3444	25	υ_{NH} (99)
4	υ_{NH}*symm.*			3595	3433	55	3603	3441	53	3592	3430	51	υ_{NH} (99)
5	υ_{NH} *peptide*	3378 s	3374 s	3531	3372	114	3510	3352	144	3502	3345	134	υ_{NH} (99)
6	υ_{NH} *symm.*	3272 m	3271 s	3477	3320	181	3470	3313	188	3469	3312	179	υ_{NH} (99)
7	υ_{CH} *asymm-pgl*	3196 m	3168 s	3143	3001	14	3146	3004	15	3148	3006	17	υ_{CH} (99)
8	υ_{CH} *asymm-asn*	2992vw	2996vs	3132	2991	9	3135	2994	5	3136	2995	6	υ_{CH} (100)
9	υ_{CH} *asymm-pgl*		2978vs	3130	2989	5	3131	2990	11	3132	2991	12	υ_{CH} (97)
10	υ_{CH} *symm-asn*			3082	2944	4	3083	2944	5	3088	2949	5	υ_{CH} (97)
11	υ_{CH} *symm-pgl*			3079	2941	12	3081	2942	11	3086	2947	12	υ_{CH} (97)
12	υ_{CH} *symm-pgl*		2933vs	3063	2925	12	3064	2926	13	3066	2928	14	υ_{CH} (99)
13	$\upsilon_{CH\text{-}pglu\ c^{\alpha}}$			3042	2906	24	3039	2903	30	3045	2908	22	υ_{CH} (100)
14	$\upsilon_{CH\text{-}asn\ c^{\alpha}}$			3036	2900	10	3037	2901	12	3044	2907	21	υ_{CH} (98)
15	υ_{CO}*pglu*			1806	1724	531	1845	1762	433	1846	1763	433	$\upsilon_{OC}(83) + \delta_{CCN}(3)$
16	υ_{CO}			1766	1725	390	1803	1722	315	1806	1724	312	υ_{NC} (5) + υ_{OC}(78)
17	$\upsilon_{CO\text{-}asn}$			1745	1704	415	1769	1710	334	1772	1713	336	υ_{NC} (7) + υ_{OC}(80)
18	υ_{CO}*peptide (amide-I)*	1696s	1687 m	1720	1680	191	1748	1690	163	1751	1693	158	υ_{NC} (5) + υ_{OC}(77) + δ_{CNH} (3)
19	δ_{HNH}*scis-asn·*	1649vs	1604 m	1629	1591	58	1634	1580	180	1653	1598	171	υ_{NC} (5) + δ_{HNH}(57) + δ_{CNH}(28)
20	δ_{HNH}*scis.*			1626	1589	254	1629	1575	138	1648	1594	136	υ_{NC} (3) + δ_{HNH}(57) + δ_{CNH}(27)
21	δ_{CNH} *peptide (amide-II)*	1535s		1560	1524	344	1566	1515	373	1574	1522	364	υ_{CC} (4) + υ_{CN}(30) + δ_{OCN}(3) + δ_{CNH}(51)
22	δ_{HCH} *scis-pglu*	1458vw		1507	1472	6	1513	1463	5	1528	1477	5	$\delta_{HCH}(27) + \Gamma_{HCCC}(20) + \Gamma_{HCCH}(28) + \Gamma_{NCCH}(10)$
23	δ_{HCH} *scis-asn*		1441 m	1474	1440	22	1480	1431	2	1496	1447	2	$\delta_{CCH}(8) + \delta_{HCH}(31) + \Gamma_{HCCN}(14) + \Gamma_{HCCC}(8) + \Gamma_{HCCH}(12) + \Gamma_{HCCO}(14)$
24	δ_{HCH} *scis-pglu*	1436v		1472	1438	1	1476	1427	22	1493	1443	21	$\delta_{CCH}(15) + \delta_{HCH}(30) + \Gamma_{HCCN}(18) + \Gamma_{HCCO}(18) + \Gamma_{HCCH}(3)$
25	δ_{HCC}*-pglu*			1423	1390	43	1425	1378	73	1432	1385	67	$\upsilon_{CC}(15) + \upsilon_{CN}(9) + \delta_{HCC}(18) + \Gamma_{HCCN}(4) + \Gamma_{HCCC}(3) + \Gamma_{HCC}(4)$
26	δ_{CNH} *asn*	1411v		1417	1384	58	1424	1377	40	1432	1385	37	υ_{NC} (16) + υ_{OC}(4) + δ_{CNH} (42) + Γ_{HCNH}(4)
27	υ_{CN}			1391	1359	136	1398	1351	107	1404	1357	118	υ_{CC} (11) + υ_{CN}(21) + δ_{CNH} (15) + δ_{CCH} (5) + δ_{OCC} (3) + δ_{OCN} (4) + δ_{HNH} (4) + Γ_{HCCC}(4) + Γ_{HCCH}(10)
28	δ_{CCH} *pglu*		1340w	1374	1343	15	1376	1330	13	1384	1338	11	υ_{NC} (5) + $\delta_{CCH}(19) + \Gamma_{HCCC}(11) + \Gamma_{NCCH}(5) + \Gamma_{HCCH}(12)$
29	δ_{CNH}			1369	1337	6	1372	1327	7	1381	1335	6	$\upsilon_{NC}(10) + \delta_{CNH}(11) + \delta_{CCH}(6) + \Gamma_{HCCH}(5) + \Gamma_{CCCH}(4) + \Gamma_{OCCH}(7) + \Gamma_{NCCH}(9)$
30	δ_{CCH}*pglu*	1306vw		1343	1312	17	1351	1307	19	1360	1315	20	$\upsilon_{NC}(3) + \delta_{CNH}(5) + \delta_{CCH}(21) + \Gamma_{CCCH}(9) + \Gamma_{HCCH}(26) + \Gamma_{OCCH}(4) + \Gamma_{NCCH}(4)$
31	δ_{CCH}*pglu*			1326	1296	50	1328	1284	27	1337	1293	8	$\upsilon_{NC}(6) + \upsilon_{CC}(8) + \delta_{CCH}(22) + \Gamma_{HCCH}(11) + \Gamma_{HCNH}(6) + \Gamma_{HCNC}(7) + \Gamma_{HCCC}(4)$
32	$\upsilon_{NC+}\delta_{CCH}$*asn*			1325	1294	40	1326	1283	63	1335	1291	81	$\upsilon_{NC}(24) + \delta_{CCH}(17) + \delta_{OCN}(3) + \delta_{HCN}(8) + \Gamma_{HCNH}(3) + \Gamma_{HCNC}(4) + \Gamma_{HCCH}(6)$
33	δ_{CNH}*peptide*		1282w	1314	1283	21	1319	1275	16	1325	1282	17	$\upsilon_{NC}(5) + \delta_{HCN}(3) + \delta_{CCH}(25) + \Gamma_{HCCC}(4) + \Gamma_{NCCH}(4) + \Gamma_{HCCH}(3)$
34	δ_{CCH}*wagg-pgl*	1268 m	1253w	1293	1263	19	1296	1253	21	1305	1262	24	$\upsilon_{CC}(8) + \upsilon_{CN}(13) + \delta_{CNH}(6) + \delta_{CCH}(25)$
35	δ_{CCH}*wagg.-asn*	1246vw		1276	1247	68	1279	1237	66	1288	1246	67	$\upsilon_{CC}(3) + \upsilon_{CN}(11) + \delta_{CNH}(7) + \delta_{CCH}(30) + \Gamma_{HCCH}(4) + \Gamma_{HCCN}(3) + \Gamma_{OCCH}(3)$
36	υ_{CN}*pglu*			1262	1233	129	1262	1220	105	1269	1227	114	υ_{CC} (6) + υ_{CN}(23) + δ_{CNH} (4) + δ_{OCN} (4) + δ_{CCH} (18) + δ_{OCC} (5) + Γ_{HCNH}(3) + Γ_{OCCH}(4) + Γ_{NCCH}(3)
37	δ_{CCH}*twist.-pgl*	1203v	1200w	1227	1199	15	1227	1186	19	1234	1193	21	$\upsilon_{CC}(8) + \delta_{CNH}(4) + \delta_{CCH}(33) + \Gamma_{NCCH}(9) + \Gamma_{OCCH}(3) + \Gamma_{HCCH}(5) + \Gamma_{CCCH}(5)$
38	δ_{CCH} *twist-asn*			1216	1188	18	1218	1178	13	1228	1187	15	$\delta_{CNH}(7) + \delta_{CCH}(38) + \Gamma_{NCCH}(5) + \Gamma_{HCNH}(3) + \Gamma_{HCCH}(4) + \Gamma_{OCCH}(4)$
39	δ_{CCH} *twist-pgl*	1130v	1137vs	1166	1139	27	1168	1130	29	1176	1137	32	$\upsilon_{CC}(5) + \delta_{CCH}(39) + \Gamma_{NCCH}(3) + \Gamma_{CCCH}(16)$
40	$\upsilon_{NC+}\delta_{CNH}$			1144	1117	2	1155	1117	2	1162	1124	2	$\upsilon_{NC}(25) + \upsilon_{CC}(20) + \upsilon_{OC}(5) + \delta_{CNH}(15) + \delta_{NCC}(3) + \delta_{CCH}$ (3)
41	$\delta_{CNH+}\upsilon_{NC}$			1127	1101	3	1134	1097	1	1139	1101	1	υ_{NC} (29) + υ_{CC} (10) + υ_{OC} (7) + δ_{CNH}(41)
42	υ_{NC}*pglu*			1111	1085	12	1114	1077	12	1118	1081	10	υ_{NC} (40) + υ_{CC} (13) + δ_{CNC}(4) + δ_{CNH}(8)
43	δ_{CNH}	1072v		1106	1081	6	1110	1073	4	1115	1078	6	υ_{NC} (25) + υ_{CC} (8) + $\delta_{CNC}(3) + \delta_{CNH}(39)$

Table 4 (continued)

	Assign.	IR	Raman	DFT-RB3LYP 6-31G++(d,p)			DFT-RB3LYP 6-31G(d,p)			DFT-RB3LYP 6-31G(d)			†TED-MONOMER DFT-RB3LYP 6-31G++(d,p)
		υ_{exp}	υ_{exp}	υ_{cal}	*υ_{scaled}	*IRint.*	υ_{cal}	*υ_{scaled}	*IR int.*	υ_{cal}	*υ_{scaled}	*IR int.*	
44	$\upsilon_{NC}+\delta_{CNH}$	1046v		1057	1033	7	1062	1027	7	1069	1034	9	υ_{NC} (14) + υ_{CC} (13) + δ_{CNC}(3) + δ_{CNH}(12) + δ_{CCH}(10)
45	$\rho(CH_2)_{pglu}$	1017v	1014 m	1047	1023	6	1052	1017	6	1058	1024	6	υ_{NC}(4) + δ_{CCH}(10) + Γ_{CCCH}(3) + Γ_{NCCC}(4) + Γ_{HCCH}(27)+ Γ_{CCCC}(6) + Γ_{CCCH}(3)
46	υ_{CC}*pglu*	980 m	987w	1017	994	5	1018	984	6	1020	987	6	υ_{NC} (10) + υ_{CC} (48)
47	υ_{CC}*pglu*			989	966	1	992	959	1	995	962	1	υ_{NC} (4) + υ_{CC} (59)
48	υ_{CC}*asn.*	932v	947 m	944	923	4	945	914	7	949	918	7	υ_{CC} (26)
49	υ_{CC}*ring –asiym*	900v	903w	922	900	8	924	894	6	927	897	6	υ_{NC} (16) + υ_{CC} (21) + δ_{CCH}(8) + δ_{CCC}(6)
50	υ_{CC}*asn*	879v	881 m	890	870	4	892	863	4	895	866	4	υ_{NC} (8) + υ_{CC} (8) + δ_{CCH}(5) + δ_{CCC}(3) + Γ_{OCCC}(5) + Γ_{NCCH}(12)
51	υ_{CC} *ring breathing*	856vw		883	863	2	885	856	1	889	859	2	υ_{NC} (6) + υ_{CC} (26) + δ_{OCN}(4) + Γ_{OCCH}(4)
52	υ_{CC}*-asn*			861	842	0	861	832	1	863	835	1	υ_{NC} (9) + υ_{CC} (55) + δ_{CNH}(9)
53	υ_{CC}*-ring*	812vw	826w	833	814	10	833	806	11	836	809	12	υ_{CC} (27) + δ_{CCH}(3) + Γ_{OCCH}(13) + Γ_{NCCH}(7)
54	Γ_{HNCO}	774v		785	767	4	791	765	5	792	766	6	υ_{CC} (11) + δ_{OCN}(8) + Γ_{HNCO}(24)
55	Γ_{HNCO}			760	742	5	761	736	8	762	737	7	δ_{CNH}(4) + δ_{CNC}(4) + δ_{OCC}(7) + δ_{OCN}(3) + Γ_{NCCC}(3) + Γ_{HNCO}(15)
56	υ_{CC}	727v		727	710	2	733	708	3	734	710	4	υ_{CC} (12) + δ_{CCN}(4) + Γ_{OCCC}(7) + Γ_{OCCH}(3) + Γ_{NCCN}(6)+ Γ_{NCCH}(4) + Γ_{HNCO}(7) + Γ_{ONCO}(9)
57	Γ_{NCCH}	709v		718	701	13	719	696	21	721	697	23	δ_{CCN}(4) + δ_{OCN}(5) + Γ_{NCCH}(24) + Γ_{HNCO}(21)
58	Γ_{CCNH}	669v	682 m	707	691	19	712	688	14	713	690	16	υ_{CC} (3) + υ_{CN} (5) + δ_{OCC}(4) + δ_{OCN}(5) + Γ_{NCCH}(23) + Γ_{HNCO}(11)
59	Γ_{HNCO}	664v		671	656	28	679	656	46	682	659	55	δ_{OCC}(4) + δ_{CCN}(10) + Γ_{OCCH}(8) + Γ_{NCCH}(4) + Γ_{HNCO}(39)
60	Γ_{OCNH}	627v		643	629	50	657	635	48	659	637	44	υ_{CN} (5) + δ_{OCC}(14) + δ_{CCC}(4) + δ_{OCN}(16) + Γ_{OCCH}(3)+ Γ_{OCNH}(13) + Γ_{NCCH}(3)
61	Γ_{CCNH}	615vw		625	611	10	631	610	6	633	612	5	δ_{OCN}(9) + δ_{OCC}(4) + Γ_{OCNH}(14) + Γ_{HCNH}(5) + Γ_{CCNH}(27)
62	Γ_{HNCC}	579vw		611	597	19	619	599	38	621	600	42	υ_{CC} (4) + δ_{OCC}(8) + δ_{CCC}(8) + δ_{CCN}(4) + Γ_{HCCH}(4) + Γ_{HNCC}(6) + Γ_{HNCO}(5)
63	δ_{OCC}			572	559	55	581	562	51	583	564	56	υ_{CC} (6) + δ_{OCC}(24) + δ_{OCN}(10) + Γ_{HNCC}(8) + Γ_{HNCO}(4)
64	Γ_{HNCC}	542v		567	554	48	568	549	52	570	551	48	δ_{CCN}(6) + δ_{OCC}(4) + δ_{CCC}(4) + Γ_{HNCO}(12) + Γ_{HNCC}(20)+ Γ_{CCCH}(4)
65	δ_{CCN}	522vw	546w	552	540	29	555	536	33	555	537	35	δ_{CCN}(28) + δ_{CNH}(3) + δ_{OCN}(33)
66	Γ_{CCNH}	501vw	498w	507	495	71	509	493	51	514	497	115	Γ_{HNCC}(48) + Γ_{CCCO}(3) + Γ_{HCNH}(4) + Γ_{HNCO}(10)
67	Γ_{CCNH}			487	475	69	505	488	265	509	492	212	Γ_{OCCH}(15) + Γ_{NCCC}(5) + Γ_{CCNH}(52) + Γ_{HNCO}(3) + Γ_{HCCC}(3)
68	δ_{OCC}			484	473	161	488	472	9	489	473	9	υ_{CC} (9) + δ_{OCC}(25) + δ_{OCN}(16) + δ_{CNC}(5) + Γ_{CCNH}(3) + Γ_{OCCN}(4)
69	Γ_{HNCO}			481	470	22	481	465	7	481	465	7	Γ_{CCNH}(44) + Γ_{HNCO}(43)
70	δ_{OCC}		421 m	409	400	6	411	398	8	412	399	8	υ_{CC} (15) + υ_{CN} (12) + δ_{OCN}(10) + δ_{OCC}(25) + δ_{NCC}(7)
71	Γ_{HNCC}			388	379	0	386	374	0	388	375	1	υ_{CC} (10) + δ_{NCC}(16) + δ_{OCN}(4) + Γ_{CCNC}(14) + Γ_{HCCN}(24)
72	δ_{NCC}			370	362	3	369	357	3	369	356	3	υ_{CC} (10) + δ_{OCC}(14) + δ_{OCN}(9) + δ_{NCC}(56)
73	δ_{NCC}		299w	308	301	18	308	298	11	307	297	11	υ_{CN} (4) + δ_{OCN}(5) + δ_{OCC}(4) + δ_{NCC}(33) + Γ_{HCCH}(3) + Γ_{OCCC}(5) + Γ_{NCCC}(4)
74	Γ_{CCNH}			294	287	170	272	263	125	269	260	10	υ_{CC} (4) + δ_{NCC}(5) + δ_{OCC}(3) + Γ_{CCNH}(29) + Γ_{HNCO}(28)
75	Γ_{CCNH}		258w	264	258	1	267	259	63	259	250	188	υ_{CC} (9) + δ_{NCC}(6) + δ_{OCC}(5) + δ_{CCC}(3) + Γ_{CCNH}(25) + Γ_{HNCO}(21)
76	δ_{CCC}			246	240	19	248	239	19	247	239	23	δ_{NCC}(17) + δ_{OCC}(6) + δ_{CCC}(19) + Γ_{CCNH}(8) + Γ_{CNCO}(4)+ Γ_{CNCC}(9)
77	δ_{CCC}			205	201	25	212	205	26	213	206	26	δ_{CCC}(15) + δ_{NCC}(9) + Γ_{CNCC}(7) + Γ_{CCNH}(12) + Γ_{OCCN}(6)+ Γ_{OCCC}(3)
78	Γ_{CNCC}			176	172	5	180	174	4	181	175	3	δ_{CCC}(19) + δ_{NCC}(7) + Γ_{CNCC}(23) + Γ_{NCCN}(3) + Γ_{CCNH}(8)
79	δ_{NCC}			154	150	8	154	149	5	153	148	5	δ_{NCC}(26) + δ_{OCN}(4) + δ_{CCC}(4) + Γ_{OCCH}(9) + Γ_{CCCO}(8)+ Γ_{NCCC}(16) + Γ_{OCNC}(7)
80	Γ_{HCCN}			134	130	2	143	139	4	144	139	4	δ_{NCC}(8) + Γ_{CNCC}(14) + Γ_{HCCN}(21) + Γ_{OCCC}(9) + Γ_{OCCC}(9)+ Γ_{CCCH}(18) + Γ_{CCCC}(7)

Table 4 (continued)

	Assign.	IR	Raman	DFT-RB3LYP 6-31G++(d,p)			DFT-RB3LYP 6-31G(d,p)			DFT-RB3LYP 6-31G(d)			†TED-MONOMER DFT-RB3LYP 6-31G++(d,p)
		υ_{exp}	υ_{exp}	υ_{cal}	$*\upsilon_{scaled}$	*IRint.*	υ_{cal}	$*\upsilon_{scaled}$	*IR int.*	υ_{cal}	$*\upsilon_{scaled}$	*IR int.*	
81	Γ_{NCCC}			105	103	3	111	107	3	111	108	3	$\delta_{CCC}(17)+\Gamma_{OCCN}(5)+\Gamma_{OCCC}(6)+\Gamma_{OCCH}(4)+\Gamma_{NCCN}(5)+$ $\Gamma_{NCCC}(22)+\Gamma_{NCCH}(13)+\Gamma_{HCCH}(4)+\Gamma_{HCCC}(3)$
82	Γ_{HCCC}			72	70	10	71	69	6	72	69	7	$\Gamma_{NCCC}(22)+\Gamma_{HCCC}(34)+\Gamma_{CCCC}(22)+\Gamma_{NCCN}(3)$
83	Γ_{HCCC}			69	67	0	70	67	1	70	68	0	$\delta_{NCC}(18)+\Gamma_{OCCN}(4)+\Gamma_{NCCC}(15)+\Gamma_{HCCC}(27)+\Gamma_{CCCC}(16)+\Gamma_{NCCH}(5)+\Gamma_{NCCN}(4)$
84	Γ_{NCCN}			49	48	1	51	49	2	52	50	1	$\Gamma_{NCCN}(18)+\Gamma_{NCCC}(12)+\Gamma_{OCCN}(16)+\Gamma_{OCCH}(12)+$ $\Gamma_{OCCC}(10)+\Gamma_{NCCH}(11)$
85	Γ_{NCCC}			41	40	4	48	47	6	50	48	6	$\delta_{NCC}(4)+\Gamma_{CCCC}(4)+\Gamma_{CCCH}(6)+\Gamma_{OCCC}(4)+\Gamma_{NCCN}(12)+$ $\Gamma_{NCCC}(40)+\Gamma_{NCCH}(20)+\Gamma_{OCCN}(7)$
86	Γ_{NCCC}			40	39	7	42	41	1	43	41	2	$\Gamma_{NCCC}(34)+\Gamma_{OCCN}(19)+\Gamma_{OCCC}(8)+\Gamma_{HCNH}(10)+\Gamma_{CCNH}(10)$
87	Γ_{NCCC}			32	32	1	32	31	2	32	31	2	$\Gamma_{OCCC}(26)+\Gamma_{OCCH}(20)+\Gamma_{NCCC}(29)+\Gamma_{NCCH}(26)$

The encapsulation value indicated that the AVP (4–5)-NH_2 peptide was entrapped and AVP (4–5)-NH_2 peptide-loaded CS NPs were obtained successfully. The calibration curve (Fig. 8a) of the AVP (4–5)-NH_2 peptide was prepared to calculate the encapsulation efficiency of the AVP (4–5)-NH_2 peptide-loaded CS NPs. The encapsulation efficiency of the AVP (4–5)-NH_2 peptide was calculated via Eq. 1, and it was found as 99%. This result indicated that, almost all peptide was encapsulated in CS NPs. A previous study which was used of CS NPs and the other protein structures showed that molecular weights of protein structures is a key parameter for a higher encapsulation efficiency [64], and it is known that encapsulation efficiency can be increased with decreased of molecular weight. For this reason, our encapsulation efficiency result was found as very higher because of AVP (4–5)-NH_2 has a small molecular weight. On the other hand, loading capacity of the AVP (4–5)-NH_2 peptide-loaded CS NPs was calculated as 10%, from Eq. 2. This means that 10% of CS NPs' weight consists of the AVP (4–5)-NH_2 peptide and each 1 mg roughly contains 0.10 mg of the peptide.

In vitro release profile

Figure 8b shows the in vitro release profile of AVP (4–5)-NH_2 peptide-loaded CS NPs. Because of the degradation of the CS polymer, the slow diffusion of AVP (4–5)-NH_2 peptide from the polymer matrix was obtained. It is also known that CS NPs have the advantage of slow and controlled drug release, which improves drug solubility and stability, enhances efficacy, and reduces toxicity [65]. The results showed that, in first 24 h 17.23% of the peptide was released and 61.13% of AVP (4–5)-NH_2 peptide was also released at the end of the 240th hour. The in vitro release of catechin from CS NPs was found at 32% within 24 h [66]. According to the results of [66], the entrapment efficiency of the particles was calculated 60% and the in vitro release was found to be 32% over 24 h. However, in our study, the encapsulation efficiency of the AVP (4–5)-NH_2 peptide was found as 99% and the release rate was found only 17.23% in the first 24 h and we reached about 60% release rate in 10 days.

The stability and integrity of AVP (4–5)-NH_2 peptide-loaded CS NPs were checked by time of in vitro release study, and the dynamic light scattering and scanning electron microscope analysis were performed after 12nd and 24th hours of the in vitro release study. The DLS results were given in Fig. S6, and it was understood that the average particle size of the AVP (4–5)-NH_2 peptide-loaded CS NPs increased significantly, and its zeta potential value decreased. After the 12 h in vitro release study, it was found that AVP

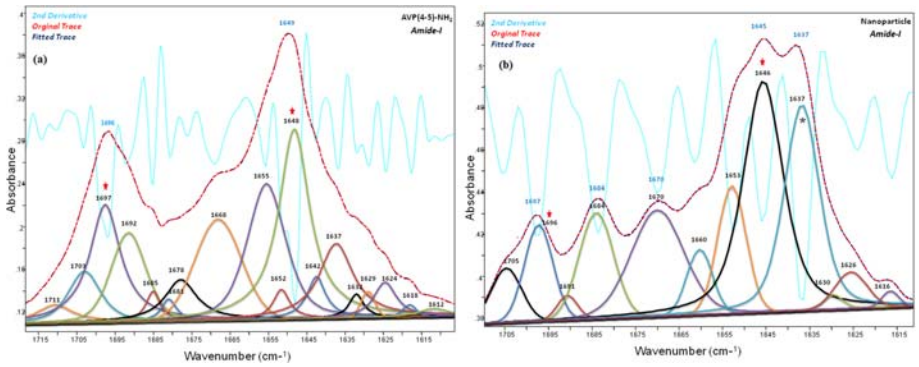

Fig. 5 The band component analysis of 1715–1610 cm^{-1}region of the Infrared spectrum of AVP (4-5)-NH_2 peptide (**a**) and AVP (4-5)-NH_2 peptide-loaded CS NPs (**b**). Chitosan bands are marked (*)

(4–5)-NH_2 peptide-loaded CS NPs had wide size distribution with 0.822, and 679.6 nm average particle size as given Fig. S6a. As seen from the Fig. S6b, the zeta potential value of AVP (4–5)-NH_2 peptide-loaded CS NPs were − 4.80 mV. Scanning electron microscope was also used to investigate the stability and integrity of the AVP (4–5)-NH_2 peptide-loaded CS NPs. SEM images of AVP (4–5)-NH_2 peptide-loaded CS NPs after 12nd hours (during in vitro release study) were given in the Fig. S7**.** According to the SEM images obtained from different perspectives, it was found that the AVP (4–5)-NH_2 peptide-loaded CS NPs were started to loose their spherical morphology. Besides, the DLS results for 24th hours were given in Fig. S8, and it was understood that the average particle size of the AVP (4–5)-NH_2 peptide-loaded CS NPs increased, and its the zeta potential value decreased. It was found that AVP (4–5)-NH_2 peptide-loaded CS NPs had wide size distribution with 0.281, and 751 nm average particle size as given Fig. S8a. As seen from the Fig. S8b, the zeta potential value of AVP (4–5)-NH_2 peptide-loaded CS NPs were − 8.65 mV. SEM images of AVP (4–5)-NH_2 peptide-loaded CS NPs after 24th hours (during in vitro release study) were given in the Fig. S9. Similarly, according to the SEM images, it was found that the AVP (4–5)-NH_2 peptide-loaded CS NPs lost more their spherical morphology. When the 12nd and 24th hour results of in vitro release study were compared, it was seen that PdI value decreased at the end of 24 h. However, in the end of the first 12nd hours PdI value was larger and the particle sizes were in two different distributions as approximately 100 nm and 679 nm. The decrease of the PdI value can be explained by increases size of the chitosan nanoparticles in the in vitro release medium and reaching 751 nm size of most of the nanoparticles after 24 h. Besides, PdI value of nanoparticles was decreased, and only one peak was observed for average particle size distribution. Moreover, zeta potential values of the AVP (4–5)-NH_2 peptide-loaded CS NPs were obtained negatively charged. It was thought that it was caused by negatively charged TPP with the degradation of the NPs. Because zeta potential values of nanoparticles increased more by the 24th hours of the in vitro release study. It was found that the AVP (4–5)-NH_2 peptide presented release profile characterized by sustained release (Fig. 8b). In the first 12 h of in vitro release study, initial release was amounted as approximately 15% of loaded peptide. This was caused by peptide which was adsorbed or weakly bound to the surface area of the CS NPs. With the 24th hours, caused by cleavage of polymer chains, release was obtained (Fig. S9).

SEM result

SEM was used to investigate the morphology of the AVP (4–5)-NH_2 peptide-loaded CS NPs. In Fig. 9, according to the

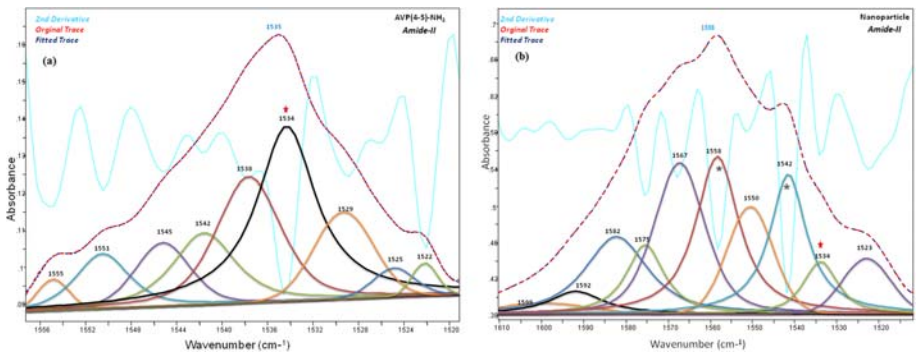

Fig. 6 The band component analysis of 1556–1520 cm^{-1}region of the Infrared spectrum of AVP (4-5)-NH_2 peptide (**a**) and AVP (4-5)-NH_2 peptide-loaded CS NPs (**b**). Chitosan bands are marked (*)

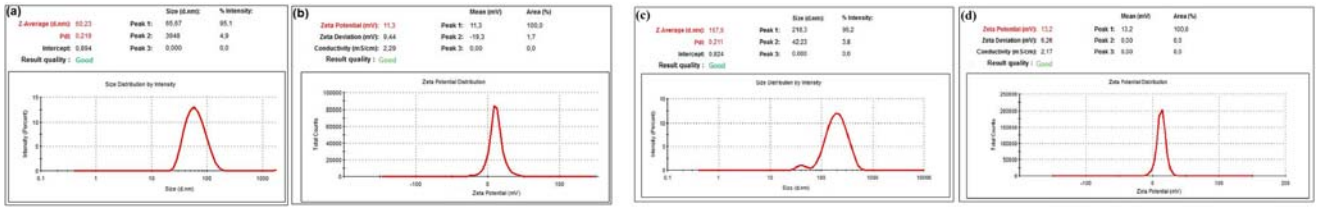

Fig. 7 Dynamic light scattering results. Size (**a**) and Zeta-potential (**b**) graphics of blank CS NPs and Size (**c**) and Zeta-potential (**d**) graphics of AVP (4–5)-NH_2 peptide-loaded CS NPs

SEM images, the AVP (4–5)-NH_2 peptide-loaded CS NPs were spherical particles with a solid dense structure.

Cytotoxicity experiments

The neuroprotective effect of AVP (4–5)-NH_2, CS NPs, and AVP (4–5)-NH_2 peptide-loaded CS NPs was performed on SH-SY5Y cells, because SH-SY5Y cells were generally used for neuroprotective assays. XTT method were applied for assay cell viability [67, 68]. Firstly, the effect dipeptide and nanoparticle formulations on growth of SH-SY5Y cells were examined and results shown in Fig. 10. As seen in Fig. 10, none of the examined formulations has toxic effect on cells. On the contrary, the formulations increased cell viability compared to the control ($p < 0.05$). This showed that AVP (4–5)-NH_2, Chitosan nanoparticles (with or without AVP(4–5)-NH_2) have neuroproliferative effect on these cells. Because AVP (4–5)-NH_2 dipeptide is a neuroprotective peptide and chitosan is a non-toxic and biocompatible polymer used for the polymeric nanoparticle structure, the obtained experimental results are consistent with the related literature results [1, 69].

Results of neuroprotective effect in vitro

In order to assay neuroprotective effect, it is necessary to treat with a damaging agent. For this purpose, cells exposed to AVP (4–5)-NH_2 peptide, CS NPs, and AVP (4–5)-NH_2 peptide-loaded CS NPs were co-treated with H_2O_2. As seen in Table 5, pretreatment with 32 μg/μL of AVP (4–5)-NH_2 peptide and CS NPs (with or without AVP (4–5)-NH_2), protected cell viability from undergoing H_2O_2–induced cell death. The evaluation of AVP (4–5)-NH_2 peptide and CS NPs in the current study indicated that they all have neuroprotective effect on SH-SY5Y neuroblastoma cell line ($p < 0,05$). There are some studies on the neuroprotective effect of chitosan in the literature [70, 71] and our findings seem to be consistent with the literature. Besides, AVP (4–5)-NH_2 is a peptide that is prominent with its neuroprotective effect in previous studies. In one of these studies, it has been shown that AVP (4–5)-NH_2 peptide in the concentration of 10^{-5} - 10^{-7} M has a neuroprotective effect against the effect of H_2O_2 on cell cultures [1]. However, HT-22 cell line was used as the cell line in their study and the effect of AVP (4–5)-NH_2 alone was investigated. Since there is no studies in literature on the encapsulation of AVP (4–5)-NH_2 peptide with CS NPs, for the first time in literature, the neuroprotective efficacy of chitosan-loaded AVP (4–5)-NH_2 was examined comparatively in this study, and it was shown that the combined effect of chitosan and AVP (4–5)-NH_2 peptide was much higher than AVP (4–5)-NH_2 peptide alone.

Conclusion

In the modelling part of our study; the experimental medium of AVP (4–5)-NH_2 peptide-loaded CS were created for the first time with in silico system and the stability of the peptide in this medium was carried out by molecular dynamics studies. To evaluate the

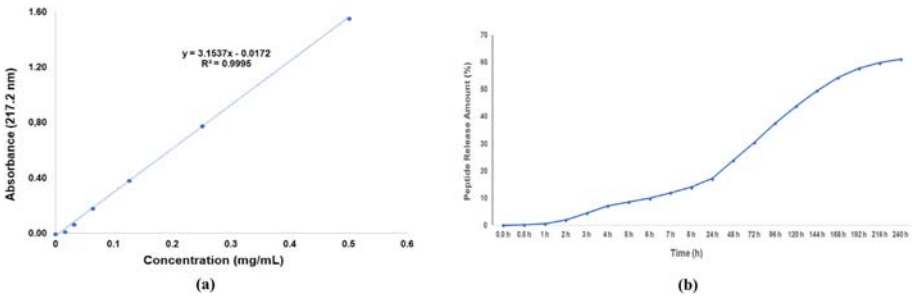

Fig. 8 Standard curve of AVP(4–5)-NH_2 peptide (**a**) and in vitro release profil of AVP(4–5)-NH_2 peptide-loaded chitosan NPs (**b**)

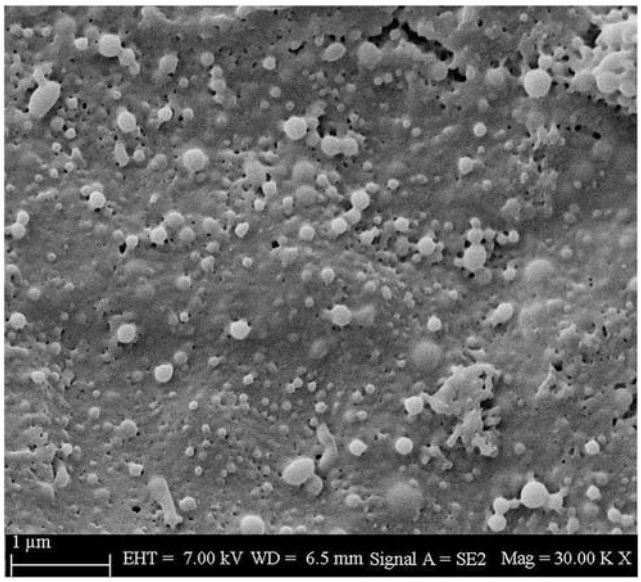

Fig. 9 SEM images of AVP(4–5)-NH_2 peptide-loaded CS NPs

molecular mechanism of AVP (4–5)-NH_2 peptide with HSP70 protein, molecular docking calculations were investigated. The active binding mechanism between peptide and protein were described using theoretical calculation methods and a potent pharmacologically features of peptide was also unveiled by ADME profile. The characteristic wavenumbers of the AVP (4–5)-NH_2 peptide were observed using IR and Raman spectra and the fundamental vibrational wavenumbers of the peptide were calculated at DFT-RB3LYP /6–31++G (d, p) basis set. Also, the assignments of the fundamental wavenumbers were assigned in accordance with the total energy distribution of the vibrational modes (TED) analysis.

In the experimental part of our study; AVP (4–5)-NH_2 peptide-loaded CS NPs was prepared by a simple and mild method of ionic gelation method to overcome low bioavailability and to increase drug effectiveness. By using dynamic light scattering (DLS), Fourier-Transform Infrared (FT-IR) spectroscopy, UV-Vis Spectrometer characterization methods, the structure of the nanoparticles were revealed. The morphology of the prepared nanoparticles was observed from SEM, and the nanoparticles were spherical form. Based on the in vitro controlled release study against PBS at pH 7.4, in first day 17.23% of the peptide was released, but 61.13% of AVP (4–5)-NH_2 peptide was released at the end of the 10th day. Neuroblastoma cells were particularly selected for the reason of AVP (4-5)-NH_2 peptide has neuroprotective effect and used in the treatment of Alzheimer's and Parkinson's disease. There is limited information about cytotoxicity of AVP (4–5)-NH_2 peptide, so we studied the cytotoxicity of AVP (4–5)-NH_2 peptide on neuroblastoma cells. CS NPs with or without AVP (4–5)-NH_2 peptide was firstly obtained in this study and their cytotoxicity were also examined. The results of cytotoxicity experiments showed that there is no cytotoxicity of AVP (4–5)-NH_2 peptide or CS NPs with the concentrations we studied. In fact, they have neuroproliferative effect on SH-SY5Y cells. Their neuroprotective effect was examined with co-treatment with H_2O_2 and consistent with the literature, AVP (4–5)-NH_2 peptide was shown as neuroprotective effect in vitro. There is no studies in literature on the encapsulation of AVP (4–5)-NH_2 peptide with CS NPs, for the first time in literature, the neuroprotective efficacy of chitosan-loaded AVP (4–5)-NH_2 was examined comparatively in this study, and it was shown that the combined effect of chitosan and AVP (4–5)-NH_2 was much higher than AVP (4–5)-NH_2 alone.

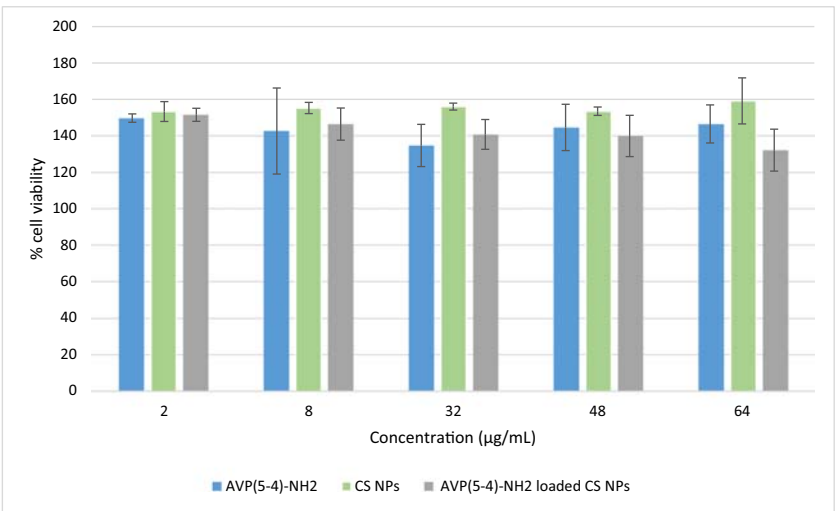

Fig. 10 Effect of AVP(4–5)-NH_2, CS NPs, and AVP(4–5)-NH_2 peptide-loaded CS NPs on cell viability of SH-SY5Y cells in vitro (Error bars indicate standard deviation)

Table 5 Neuroprotective effect of AVP(4–5)-NH_2 peptide, CS NPs, and AVP(4–5)-NH_2 peptide-loaded CS NPs on SH-SY5Y cells against H_2O_2 induced cell death (± sign indicates standard deviation)

Control- H_2O_2	AVP(5–4)-NH_2	Chitosan NPs	AVP(5–4)-NH2 loaded Chitosan NPs
53,4 ± 2,2	**73,2 ± 4,6**	**70,9 ± 3,3**	**78,3 ± 7,1**

Acknowledgements Authors are also very thankful to Rita Podzuna for allowing using the docking program with Schrödinger's Small-Molecule Drug Discovery Suite. In this study, the infrastructure of Applied Nanotechnology and Antibody Production Laboratory established with TUBITAK support (project numbers: 115S132 and 117S097) was used. Authors would thank to TUBITAK for their support.

Availability of data and materials Data sharing not applicable to this article as no datasets were generated or analysed during the current study.

Authors' contributions SG: Participated in the design of the study, carried out the FTIR, band component analysis study, molecular docking, and molecular dynamic simulation and drafted the manuscript. YBK and TZ: Participated in the design of the experimental study, (synthesize and characterize nanoparticles) drafted the manuscript. RK: Participated in the design of the experimental study (cytotoxicity studies) drafted the manuscript. BB and YK: Participated in the design of the molecular docking and molecular dynamic simulation. AO and SA: Responsible for the study design and gave final approval of the version to be published. All authors read and approved the final manuscript and provide financial and administrative support.

Funding This study was supported by the Research funds of Istanbul University [ONAP-2423].

Compliance with ethical standards

Conflict of interests On behalf of all authors, the corresponding author states that there is no conflict of interest.

Consent for publication Not applicable.

Ethics approval and consent to participate Not applicable.

References

1. Zenina TA, Gudasheva TA, Bukreyev YS, Seredenin SB. Neuroprotective effect of dipeptide AVP (4-5)-NH_2 is associated with nerve growth factor and heat shock protein HSP70. Bull Exp Biol Med. 2007;144(4):543–5.
2. Evans CG, Wisén S, Gestwicki JE. Heat shock proteins 70 and 90 inhibit early stages of amyloid beta (1-42) aggregation in vitro. J Biol Chem. 2006.
3. Kreek MJ, Zhou Y, Levran O. Functions of arginine vasopressin and its receptors: importance of human molecular genetics studies in bidirectional translational research. Biol Psychiatry. 2011;70(6):502.
4. Wolkowitz OM, Rothschild AJ. Psychoneuroendocrinology: the scientific basis of clinical practice. American psychiatric pub. 2008.
5. Batla A, Phé V, De Min L, Panicker JN. Nocturia in Parkinson's disease: why does it occur and how to manage? Movement Disorders Clinical Practice. 2016;3(5):443–51.
6. Mayer MP, Bukau B. Hsp70 chaperones: cellular functions and molecular mechanism. Cell Mol Life Sci. 2005;62(6):670.
7. Witt SN. Hsp70 molecular chaperones and Parkinson's disease. Biopolymers: Original Research on Biomolecules. 2010;93(3):218–28.
8. Lu RC, Tan MS, Wang H, Xie AM, Yu JT, Tan L. Heat shock protein 70 in Alzheimer's disease. Biomed Res Int. 2014.
9. Calzoni E, Cesaretti A, Polchi A, Di Michele A, Tancini B, Emiliani C. Biocompatible polymer nanoparticles for drug delivery applications in cancer and neurodegenerative disorder therapies. J Funct Biomater. 2019;10(1).
10. Zhao LM, Shi LE, Zhang ZL, Chen JM, Shi DD, Yang J, et al. Preparation and application of chitosan nanoparticles and nanofibers. Braz J Chem Eng. 2011;28(3):353–62.
11. Ghadi A, Mahjoub S, Tabandeh F, Talebnia F. Synthesis and optimization of chitosan nanoparticles: potential applications in nanomedicine and biomedical engineering. Caspian journal of internal medicine. 2014;5(3):156–61.
12. Landriscina A, Rosen J, Friedman AJ. Biodegradable chitosan nanoparticles in drug delivery for infectious disease. Nanomedicine. 2015;10(10):1609–19.
13. Wang X, Chi N, Tang X. Preparation of estradiol chitosan nanoparticles for improving nasal absorption and brain targeting. Eur J Pharm Biopharm. 2008;70(3):735–40.
14. Sadigh-Eteghad S, Talebi M, Farhoudi M, Mahmoudi J, Reyhani B. Effects of levodopa loaded chitosan nanoparticles on cell viability and caspase-3 expression in PC12 neural like cells. Neurosciences. 2013;18(3):281–3.
15. Frisch MJ, Trucks GW, Schlegel HB, Scuseria GE, Robb MA, Cheeseman JR, et al. Gaussian 16. Revision A. 2016;3.
16. Wang J, Wang W, Kollman PA, Case DA. Automatic atom type and bond type perception in molecular mechanical calculations. J Mol Graph Model. 2006;25(2):247–60.
17. Wang J, Wolf RM, Caldwell JW, Kollman PA, Case DA. Development and testing of a general amber force field. J Comput Chem. 2004;25(9):1157–74.
18. da Silva AWS, Vranken WF. ACPYPE-Antechamber python parser interface. BMC research notes. 2012;5(1):367.
19. Balajee R, Rajan MD. Molecular docking and simulation studies of farnesyl trasnferase with the potential inhibitor theflavin. Journal of Applied Pharmaceutical Science. 2011;1(8):141.
20. Abraham MJ, Murtola T, Schulz R, Páll S, Smith JC, Hess B, et al. GROMACS: high performance molecular simulations through multi-level parallelism from laptops to supercomputers. SoftwareX. 2015;1:19–25.
21. Hornak V, Abel R, Okur A, Strockbine B, Roitberg A, Simmerling C. Comparison of multiple Amber force fields and development of improved protein backbone parameters. Proteins: Structure, Function, and Bioinformatics. 2006;65(3):712–25.
22. Jorgensen WL, Chandrasekhar J, Madura JD, Impey RW, Klein ML. Comparison of simple potential functions for simulating liquid water. J Chem Phys. 1983;79(2):926–35.
23. Bussi G, Donadio D, Parrinello M. Canonical sampling through velocity rescaling. The Journal of Chemical Physics. 2007;126(1).
24. Parrinello M, Rahman A. Polymorphic transitions in single crystals: a new molecular dynamics method. J Appl Phys. 1981;52(12):7182–90.
25. Hess B, Bekker H, Berendsen HJ, Fraaije JG. LINCS: a linear constraint solver for molecular simulations. J Comput Chem. 1997;18(12):1463–72.
26. Turner PJ. XMGRACE, Version 5.1. 19. Center for Coastal and Land-Margin Research, Oregon Graduate Institute of Science and Technology, Beaverton, OR. 2005.

27. Humphrey W, Dalke A, Schulten K. VMD: visual molecular dynamics. J Mol Graph. 1996;14(1):33–8.
28. Sriram M, Osipiuk J, Freeman BC, Morimoto RI, Joachimiak A. Human Hsp70 molecular chaperone binds two calcium ions within the ATPase domain. Structure. 1997;5(3):403–14.
29. Bienert S, Waterhouse A, de Beer TA, Tauriello G, Studer G, Bordoli L, et al. The SWISS-MODEL repository—new features and functionality. Nucleic Acids Res. 2016;45(D1):D313–9.
30. Friesner RA, Murphy RB, Repasky MP, Frye LL, Greenwood JR, Halgren TA, et al. Extra precision glide: docking and scoring incorporating a model of hydrophobic enclosure for protein− ligand complexes. J Med Chem. 2006;49(21):6177–96.
31. Halgren TA, Murphy RB, Friesner RA, Beard HS, Frye LL, Pollard WT, et al. Glide: a new approach for rapid, accurate docking and scoring. 2. Enrichment factors in database screening. J Med Chem. 2004;47(7):1750–9.
32. Friesner RA, Banks JL, Murphy RB, Halgren TA, Klicic JJ, Mainz DT, et al. Glide: a new approach for rapid, accurate docking and scoring. 1. Method and assessment of docking accuracy. J Med Chem. 2004;47(7):1739–49.
33. Harder E, Damm W, Maple J, Wu C, Reboul M, Xiang JY, et al. OPLS3: a force field providing broad coverage of drug-like small molecules and proteins. J Chem Theory Comput. 2015;12(1):281–96.
34. Sastry GM, Adzhigirey M, Day T, Annabhimoju R, Sherman W. Protein and ligand preparation: parameters, protocols, and influence on virtual screening enrichments. J Comput Aided Mol Des. 2013;27(3):221–34.
35. Søndergaard CR, Olsson MH, Rostkowski M, Jensen JH. Improved treatment of ligands and coupling effects in empirical calculation and rationalization of p K a values. J Chem Theory Comput. 2011;7(7):2284–95.
36. Venkatesan A, Rambabu M, Jayanthi S. Febin Prabhu Dass J. Pharmacophore feature prediction and molecular docking approach to identify novel anti-HCV protease inhibitors. J Cell Biochem. 2018;119(1):960–6.
37. Divya K, Jisha MS. Chitosan nanoparticles preparation and applications. Environ Chem Lett. 2018;16(1):101–12.
38. Sullivan DJ, Cruz-Romero M, Collins T, Cummins E, Kerry JP, Morris MA. Synthesis of monodisperse chitosan nanoparticles. Food Hydrocoll. 2018;83:355–64.
39. Ahsan SM, Thomas M, Reddy KK, Sooraparaju SG, Asthana A, Bhatnagar I. Chitosan as biomaterial in drug delivery and tissue engineering. Int J Biol Macromol. 2018;110:97–109.
40. Kilinc YB, Akdeste ZM, Koc RC, Bagirova M, Allahverdiyev A. Synthesis and characterization of antigenic influenza a M2e protein peptide-poly (acrylic) acid bioconjugate and determination of toxicity in vitro. Bioengineered. 2014;5(6):357–62.
41. Erci F, Cakir-Koc R, Isildak I. Green synthesis of silver nanoparticles using Thymbra spicata L. var. spicata (zahter) aqueous leaf extract and evaluation of their morphology-dependent antibacterial and cytotoxic activity. Artificial Cells, Nanomedicine, and Biotechnology. 2018;46:150–8.
42. Liwo A, Tempczyk A, Oldziej S, Shenderovich MD, Hruby VJ, Talluri S, et al. Exploration of the conformational space of oxytocin and arginine-vasopressin using the electrostatically driven Monte Carlo and molecular dynamics methods. Biopolymers. 1996;38(2):157–75.
43. Schmidt JM, Ohlenschläger O, Rüterjans H, Grzonka Z, Kojro E, Pavo I, et al. Conformation of [8-arginine] vasopressin and V1 antagonists in dimethyl sulfoxide solution derived from two-dimensional NMR spectroscopy and molecular dynamics simulation. Eur J Biochem. 1991;201(2):355–71.
44. Lipinski CA, Lombardo F, Dominy BW, Feeney PJ. Experimental and computational approaches to estimate solubility and permeability in drug discovery and development settings. Adv Drug Deliv Rev. 1997;23(1–3):3–25.
45. Lipinski CA. Lead-and drug-like compounds: the rule-of-five revolution. Drug Discov Today Technol. 2004;1(4):337–41.
46. Leo A, Hansch C, Elkins D. Partition coefficients and their uses. Chem Rev. 1971;71(6):525–616.
47. Tihanyi K, Vastag M (Eds.). Solubility, delivery and ADME problems of drugs and drug-candidates. Bentham Science Publishers. 2011.
48. Veber DF, Johnson SR, Cheng HY, Smith BR, Ward KW, Kopple KD. Molecular properties that influence the oral bioavailability of drug candidates. J Med Chem. 2002;45(12):2615–23.
49. Johansen A, Hansen HD, Svarer C, Lehel S, Leth-Petersen S, Kristensen JL, et al. The importance of small polar radiometabolites in molecular neuroimaging: a PET study with [11C] Cimbi-36 labeled in two positions. J Cereb Blood Flow Metab. 2018;38(4):659–68.
50. Carpenter TS, Kirshner DA, Lau EY, Wong SE, Nilmeier JP, Lightstone FC. A method to predict blood-brain barrier permeability of drug-like compounds using molecular dynamics simulations. Biophys J. 2014;107(3):630–41.
51. Dressman JB, Lennernas H. Oral drug absorption: prediction and assessment: CRC Press; 2000.
52. Mohammadpour Dounighi N, Eskandari R, Avadi MR, Zolfagharian H. Mir Mohammad Sadeghi a, Rezayat M. preparation and in vitro characterization of chitosan nanoparticles containing Mesobuthus eupeus scorpion venom as an antigen delivery system. Journal of Venomous Animals and Toxins Including Tropical Diseases. 2012;18(1):44–52.
53. Anicuta SG, Dobre L, Stroescu M, Jipa I. Fourier transform infrared (FTIR) spectroscopy for characterization of antimicrobial films containing chitosan. Analele Universită Ńii din Oradea Fascicula: Ecotoxicologie, Zootehnie şi Tehnologii de Industrie Alimentară. 2010:1234–40.
54. Liu CG, Desai KGH, Chen XG, Park HJ. Preparation and characterization of nanoparticles containing trypsin based on hydrophobically modified chitosan. J Agric Food Chem. 2005;53(5):1728–33.
55. Negrea P, Caunii A, Sarac I, Butnariu M. The study of infrared spectrum of chitin and chitosan extract as potential sources of biomass. Digest Journal of Nanomaterials & Biostructures (DJNB). 2015;10(4).
56. Silva SM, Braga CR, Fook MV, Raposo CM, Carvalho LH, Canedo EL. Application of infrared spectroscopy to analysis of chitosan/clay nanocomposites. In Infrared Spectroscopy-Materials Science, Engineering and Technology. InTech. (2012).
57. Mazancová P, Némethová V, Treľová D, Kleščíková L, Lacík I, Rázga F. Dissociation of chitosan/tripolyphosphate complexes into separate components upon pH elevation. Carbohydr Polym. 2018;192:104–10.
58. PQS version 3.1, Parallel Quantum Solutions, 2013 Green Acres Road, Suite A Fayetteville, Arkansas, 72703 USA.
59. Balci K, Akyuz S. A vibrational spectroscopic investigation on benzocaine molecule. Vib Spectrosc. 2008;48(2):215–28.
60. Murdock RC, Braydich-Stolle L, Schrand AM, Schlager JJ, Hussain SM. Characterization of nanomaterial dispersion in solution prior to in vitro exposure using dynamic light scattering technique. Toxicol Sci. 2008;101(2):239–53.
61. Patil P, Bhoskar M. Optimization and evaluation of spray dried chitosan nanoparticles containing doxorubicin. Int J Curr Pharm Res. 2014;6(1):7–15.
62. Hu YL. Qi W, Han F, Shao JZ. Gao JQ Toxicity evaluation of biodegradable chitosan nanoparticles using a zebrafish embryo model International journal of nanomedicine. 2011;6:3351.

63. Tang ZX, Qian JQ, Shi LE. Preparation of chitosan nanoparticles as carrier for immobilized enzyme. Appl Biochem Biotechnol. 2007;136(1):77–96.
64. Jarudilokkul S, Tongthammachat A, Boonamnuayvittaya V. Preparation of chitosan nanoparticles for encapsulation and release of protein. Korean J Chem Eng. 2011;28(5):1247.
65. Wang JJ, Zeng ZW, Xiao RZ, Xie T, Zhou GL, Zhan XR, et al. Recent advances of chitosan nanoparticles as drug carriers. Int J Nanomedicine. 2011;6:765.
66. Dudhani AR, Kosaraju SL. Bioadhesive chitosan nanoparticles: preparation and characterization. Carbohydr Polym. 2010;81(2): 243–51.
67. Huyck L, Ampe C, Van Troys M. The XTT cell proliferation assay applied to cell layers embedded in three-dimensional matrix. Assay and drug development technologies. 2012;10(4):382–92.
68. López-García J, Lehocký M, Humpolíček P, Sáha P. HaCaT keratinocytes response on antimicrobial atelocollagen substrates: extent of cytotoxicity, cell viability and proliferation. Journal of functional biomaterials. 2014;5(2):43–57.
69. Zhao D, Yu S, Sun B, Gao S, Guo S, Zhao K. Biomedical applications of chitosan and its derivative nanoparticles. Polymers. 2018;10(4):462.
70. Cho Y, Shi R, Borgens RB. Chitosan nanoparticle-based neuronal membrane sealing and neuroprotection following acrolein-induced cell injury. J Biol Eng. 2010;4(1):2.
71. Pangestuti R, Kim SK. Neuroprotective properties of chitosan and its derivatives. Marine Drugs. 2010;8(7):2117–28.